Ore Geology Reviews 104 (2019) 190–207

Contents lists available at ScienceDirect

Ore Geology Reviews

journal homepage: www.elsevier.com/locate/oregeorev

# The Yinachang Fe-Cu-Au-U-REE deposit and its relationship with intermediate to mafic intrusions, SW China: Implications for ore genesis and geodynamic setting

Ligang Zhu[a,b,d], Jiajun Liu[a,b,*], Leon Bagas[a,c,d,*], Emmanuel John M. Carranza[e,f], Degao Zhai[a,b], Guangzhi Meng[g], Jianping Wang[a,b], Yinhong Wang[a,b], Fangfang Zhang[a,b], Zhenjiang Liu[a,b]

[a] State Key Laboratory of Geological Processes and Mineral Resources, China University of Geosciences, Beijing 100083, China
[b] School of Earth Science and Resources, China University of Geosciences (Beijing), Beijing 100083, China
[c] MLR Key Laboratory of Metallogeny and Mineral Assessment, Institute of Mineral Resources, Chinese Academy of Geological Sciences, Beijing 100037, China
[d] Centre for Exploration Targeting, University of Western Australia, Perth, WA 6009, Australia
[e] Geological Geosciences, School of Agricultural, Earth and Environmental Sciences, University of KwaZulu-Natal, Durban 4041, South Africa
[f] Economic Geology Research Centre (EGRU), James Cook University, Townsville, QLD 4811, Australia
[g] Geological Team 306, Yunnan Bureau of Nonferrous Geology, Kunming 650217, China

ARTICLE INFO

*Keywords:*
Columbia supercontinent
Yangtze block
Kangdian region
Yinachang deposit
LA-ICP-MS zircon U-Pb dating
Zircon trace element analysis

ABSTRACT

The Yinachang Fe-Cu-Au-U-REE deposit is located in the Kangdian region at the southwestern margin of the Yangtze Block. This contribution presents petrological, geochronological, whole rock geochemical, and Rare Earth Elements (REE) geochemistry of zircons of gabbro and diorite dykes associated with the Yinachang Fe-Cu-Au-U-REE deposit, aiming to constrain the age of the mineralisation and help refine our understanding of the tectonic setting of the region. Zircons from diorite have a Palaeoproterozoic U-Pb age of 2014 ± 30 Ma, and zircons from the gabbro could not be dated because they are metamict, having a high concentration of uranium. The ca. 2014 Ma age of the zircons in the diorite indicates that the southwestern part of the Yangtze Block is partly synchronous with the Columbia Supercontinent. Geochemically, the diorite and gabbro are enriched in large-ion lithophile elements (LILEs) such as Rb and U, and depleted in high-field-strength elements (HFSEs) such as Nb, P, Ti, Ba, and Sr. The diorite is enriched in light REEs (LREEs) and has a slight to negligible Eu anomaly, which are characteristic of ocean-island basalts containing mantle-derived high potassic calc-alkaline rocks. In contrast, the gabbro is weakly enriched in LREEs and has a slightly negative Eu anomaly similar to those of potassic calc-alkaline enriched mid-ocean-ridge basalt. The average combined REE content of zircons from the gabbro is 19401 ppm and is significantly higher than that of the zircons from the diorite averaging 1020 ppm. This indicates that the gabbro is closely related with the REE mineralisation at the deposit. The geochemistry of the diorite indicates that it formed at the continental margin of a volcanic-arc. It also indicates that the magmatic rocks in the region have a possible mantle plume origin contaminated by crustal material and located at a transitional zone between a rift and an ocean-continent tectonic setting.

## 1. Introduction

The Yangtze Block is separated from the North China Block by the Qinlin-Dabie-Sulu Orogen to the north, and is bounded to the southwest by the Tibetan Plateau and southeast by the Cathaysia Block (Fig. 1a). Metamorphosed Palaeo- to Mesoproterozoic sedimentary and volcanic rocks host Fe-Cu-REE-Pb-Zn deposits along the western margin of the Yangtze Block (Fig. 1b; Yang et al., 2012, 2014). Examples are found in the Kangdian region that includes the Lala Fe-Cu deposit in northern Sichuan Province, the Yinachang Fe-Cu-Au-U-REE and E'touchang Fe (-Cu) deposits in central Yunnan Province, and the Dahongshan Fe-Cu deposit in southern Yunnan Province. These deposits are characterised by complex and multiple deformation and metamorphism (Greentree and Li, 2008).

These mineral systems in the Kangdian region are locally termed as the Dahongshan-, Xikuangshan- and E'touchang-type Fe-Cu deposits, and the Yimen-, Fengshan-, Taoyuan-, and Lala types of Cu deposits. The presence of these deposits in the region makes it an important

* Corresponding authors at: State Key Laboratory of Geological Processes and Mineral Resources, China University of Geosciences, Beijing 100083, China.
*E-mail addresses:* liujiajun@cugb.edu.cn (J. Liu), leon.bagas@me.com (L. Bagas).

https://doi.org/10.1016/j.oregeorev.2018.11.005
Received 10 July 2018; Received in revised form 2 November 2018; Accepted 6 November 2018
Available online 09 November 2018
0169-1368/ 

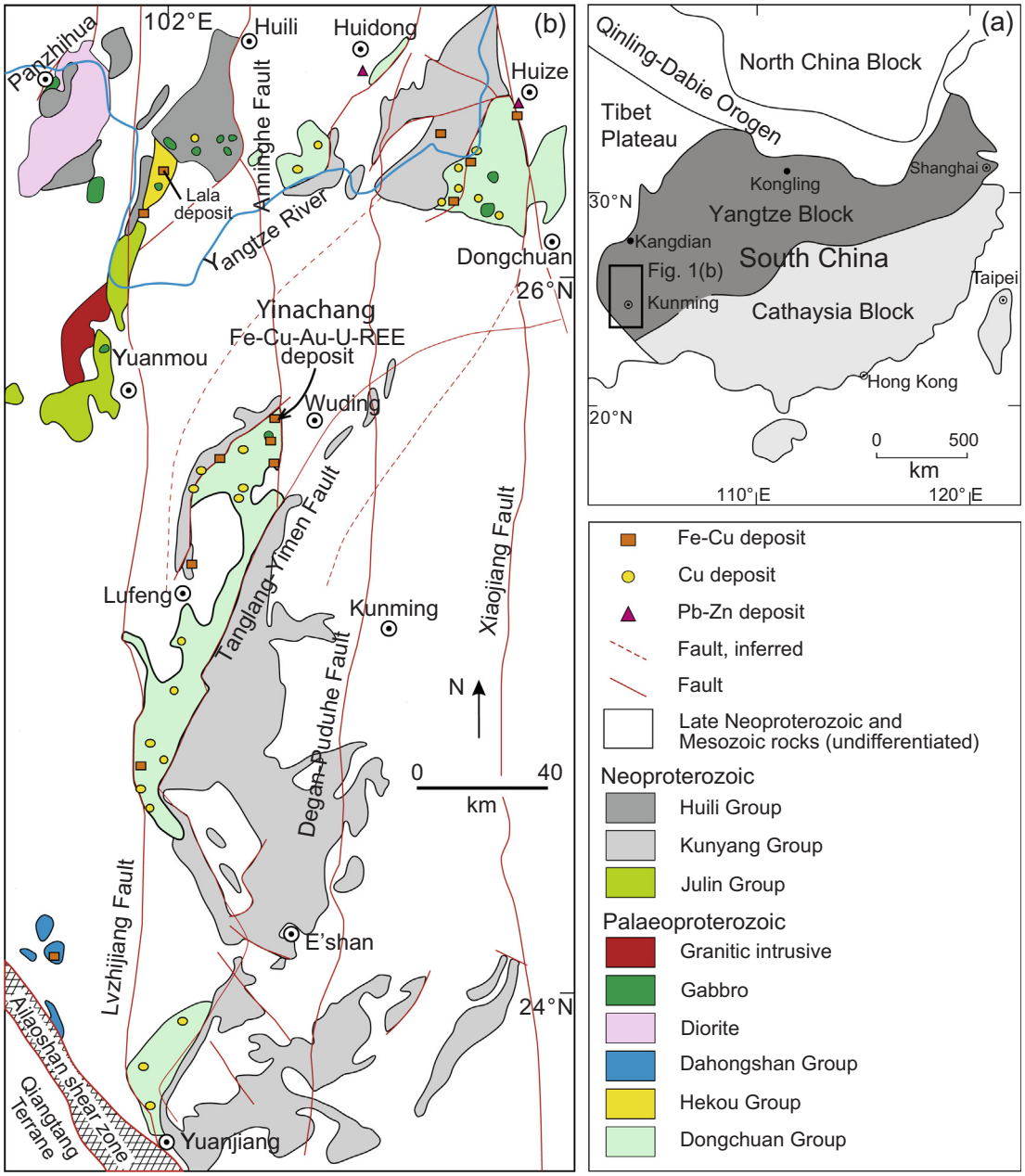


**Fig. 1.** Location of: (a) the Kangdian region, South China; and (b) southwestern Yangtze Block (after Chen et al., 2013).

source for polymetallic commodities in China (c.f. Zhao and Zhou, 2011; Zhao et al., 2012, 2013a).

The Fe–Cu deposits hosted by Palaeoproterozoic volcanic sedimentary rocks in the Kangdian region are interpreted as volcanic-hosted massive sulphide-type deposits related to volcanic eruptions (e.g. Qian and Shen, 1990; Sun et al., 1991). However, these deposits differ from volcanic-hosted massive sulphide-type deposits in terms of tectonic setting, mineral compositions, iron-oxides (i.e. $Fe^{2+}$ or $Fe^{3+}$), textures, and relationship with the country rocks.

The Lala, Xikuangshan, Yinachang and Dahongshan deposits have been recently classified as iron-oxide copper-gold (IOCG) type deposits (e.g. Li et al., 2002; Fang et al., 2013; Fang, 2014; Hou et al., 2015b). This interpretation places the genesis of the deposits in a common tectonic setting associated with Palaeoproterozoic magmatism (Zhao et al., 2010; Wang et al., 2013a; Fang, 2014). The tectonic and related magmatic events are broadly synchronous with plate convergence in the Columbia or Nuna Supercontinent (Chen et al., 2013; Fan et al., 2013; Zhao et al., 2013b; Zhou et al., 2014). The supercontinent is thought to have been assembled during global-scale Palaeoproterozoic collisional (ca. 2100–1800 Ma) events, and included Amazonia, Australia, Baltica, Kalaharia, Laurentia, North China, Siberia, and Ukrainia (Rogers and Santosh, 2002; Evans and Mitchell, 2011; Pesonen et al., 2012; Zhang et al., 2012; Deng et al., 2013a,b).

Most IOCG deposits are spatially associated and coeval with regional intrusive activity (e.g. Williams et al., 2005; Corriveau and Mumin, 2010; Groves et al., 2010). However, the relationships between the gabbro, diorite and the Yinachang Fe-Cu-Au-U-REE deposit remain uncertain, and the genesis of the mineralisation is not adequately understood due to limited detailed geological and geochemical data. In addition, the Yinachang deposit has a unique mineral assemblage rich in REEs, unlike typical IOCG deposits, and has thus attracted geological interest in China (e.g. Yang et al., 2004, 2005; Hou et al., 2013, 2015a; Ye et al., 2013; Li et al., 2015; Zhao et al., 2015).

This contribution presents new geological, geochemical and geochronology evidence that allows us to better understand the genesis of the Yinachang deposit. The techniques used are scanning electron

**Table 1**
Dates from Palaeo- to Mesoproterozoic units and magmatic rocks in the Kangdian region.

| No. | Unit | Lithology | Dating technique | Age | ± | Reference |
|---|---|---|---|---|---|---|
| 1 | Dahongshan Gp | Schistose tuff | SHRIMP zircon U-Pb | 1675 | 8 | Greentree and Li (2008) |
| 2 | Dahongshan Gp | Felsic volcanic | LA-ICP-MS Zircon U-Pb | 1681 | 13 | Zhao and Zhou (2011) |
| 3 | Dahongshan Gp | Meta-felsic volcanic | LA-ICP-MS Zircon U-Pb | 1711 | 4 | Yang et al. (2012) |
| 4 | Dahongshan Gp | Mafic granulite | LA-ICP-MS Zircon U-Pb | 1686 | 4 | Yang et al. (2012) |
| 5 | Dahongshan Gp | Dolerite dyke | LA-ICP-MS Zircon U-Pb | 1659 | 16 | Zhao and Zhou (2011) |
| 6 | Dahongshan Gp | Natritie-bearing vesicular lava | TIMS zircon U-Pb | 1672 | 8 | Hu et al. (1991) |
| 7 | Dahongshan Gp | Intermediate sodic lava (keratophyre) | Whole rock Sm-Nd isochron | 1657 | 82 | Hu et al. (1991) |
| 8 | Hekou Gp | Intermediate sodic lava (keratophyre) | SHRIMP zircon U-Pb | 1695 | 20 | He (2009) |
| 9 | Hekou Gp | Gabbro | SHRIMP zircon U-Pb | 1710 | 8 | Guan et al. (2011) |
| 10 | Hekou Gp | Gabbro | LA-ICP-MS zircon U-Pb | 1657 | 21 | Chen et al. (2013) |
| 11 | Hekou Gp | Meta-tuff | LA-ICP-MS zircon U-Pb | 1705 | 6 | Chen et al. (2013) |
| 12 | Hekou Gp | Meta-tuff | LA-ICP-MS zircon U-Pb | 1708 | 7 | Chen et al. (2013) |
| 13 | Hekou Gp | Meta-tuff | LA-ICP-MS zircon U-Pb | 1697 | 13 | Chen et al. (2013) |
| 14 | Lower Kunyang Gp | Tuff | LA-ICP-MS zircon U-Pb | 1742 | 13 | Zhao et al. (2010) |
| 15 | Lower Kunyang Gp | Tuffaceous volcanic | SHRIMP zircon U-Pb | 1503 | 17 | Sun et al. (2009) |
| 16 | Lower Kunyang Gp | Porphyritic granite | LA-ICP-MS zircon U-Pb | 1730 | 15 | Wang et al. (2013c) |
| 17 | Lower Kunyang Gp | Dolerite dyke | LA-ICP-MS zircon U-Pb | 1767 | 15 | Guo et al. (2014a) |
| 18 | Lower Kunyang Gp | Magmatic breccia | LA-ICP-MS zircon U-Pb | 1739 | 13 | Hou et al. (2013) |
| 19 | Lower Kunyang Gp | Dolerite dyke | SHRIMP zircon U-Pb | 1676 | 15 | Zhu et al. (2011) |
| 20 | Lower Kunyang Gp | Dolerite dyke | LA-ICP-MS zircon U-Pb | 1690 | 32 | Zhao et al. (2010) |
| 21 | Lower Kunyang Gp | Dolomite | Whole rock Pb-Pb isochron | 1716 | 56 | Chang and Zhu (2002) |
| 22 | Lower Kunyang Gp | Carbonaceous slate | Whole-rock Pb-Pb isochron | 1607 | 128 | Chang and Zhu (2002) |
| 23 | Upper Kunyang Gp | Tuff | SHRIMP zircon U-Pb | 1142 | 16 | Greentree et al. (2006) |
| 24 | Upper Kunyang Gp | Tuff | SHRIMP zircon U-Pb | 995 | 15 | Greentree et al. (2006) |
| 25 | Upper Kunyang Gp | Tuff | SHRIMP zircon U-Pb | 1032 | 9 | Zhang et al. (2007) |
| 26 | Upper Kunyang Gp | Carbonaceous slate | Whole-rock Pb-Pb isochron | 1258 | 70 | Chang and Zhu (2002) |
| 27 | Huili Gp | Anorthosite | TIMS Zircon U-Pb | 958 | 16 | Mou et al. (2003) |
| 28 | Huili Gp | Meta-rhyolite | SHRIMP zircon U-Pb | 1028 | 9 | Geng et al. (2007) |
| 29 | Huili Gp | Gabbro | LA-ICP-MS zircon U-Pb | 1694 | 16 | Wang et al. (2013a) |
| 30 | Huili Gp | Gabbro | TIMS Zircon U-Pb | 1494 | 6 | Fan et al. (2013) |
| 31 | Huili Gp | Gabbro | TIMS Baddeleyite U-Pb | 1486 | 3 | Fan et al. (2013) |
| 32 | Huili Gp | Gabbro | TIMS Baddeleyite U-Pb | 1490 | 4 | Fan et al. (2013) |
| 33 | Huili Gp | Gabbro & diorite | LA-ICP-MS zircon U-Pb | 1513 | 13 | Geng et al. (2012) |

microscope, whole-rock geochemistry, laser ablation–inductively coupled plasma–mass spectrometry (LA-ICP-MS) U-Pb zircon dating, and zircon REE analyses. It is anticipated that the results of this study will further promote studies of the tectonic setting of Palaeoproterozoic magmatism, tectonics, and the interaction between the crust and mantle along the western margin of the Yangtze Block.

## 2. Geological setting

### 2.1. Regional geology

The Kangdian region is located along the western edge of the Yangtze Block between the Lvzhijiang and Xiaojiang faults (Fig. 1b). The oldest units in the region are metamorphosed Palaeo- to Mesoproterozoic clastic sedimentary, mafic and felsic volcanic, and magmatic rocks (Fig. 1b). The supracrustal rocks are assigned to the ca. 1700–1600 Ma Dahongshan, Dongchuan (also known as the Lower Kunyang Group), ca. 1700–1600 Ma Hekou, ca. 1700–1000 Ma Huili, and ca. 1300–1000 Ma Upper Kunyang groups (Table 1).

The widespread mafic to felsic volcanic, and magmatic rocks in the Kangdian region are interpreted to be rift-related and include rhyolite, basalt, gabbro, andesite, and granite. The tectonic structures in the region trend northwards, and large-scale faults host mafic, mafic to felsic intrusive bodies, volcanic centres, and many mineral deposits. Such faults include the Anninghe, Xiaojiang, Lvzhijiang, Degan-Puduhe, and Tanglang-Yimen faults (Fig. 1b).

The Dahongshan Group includes the Manganghe Formation, which hosts the Dahongshan Fe-Cu deposit. The formation is intruded by dolerite and gabbro dykes and small bodies (stocks) that are variably metamorphosed. One of the dolerite dykes in the area has a Laser Ablation-Inductively Coupled Plasma-Mass Spectrometry (LA-ICP-MS) zircon age of 1659 ± 16 Ma (Zhao and Zhou, 2011).

The Hekou Group consists of metamorphic volcanic and sedimentary rocks and hosts the Lala Fe-Cu deposit. Quartz keratophyre is present in the lower part of the group, which is overlain by fine-grained basalt. Gabbroic and doleritic dykes and stocks are present in the Hekou area of the Huili Country. One of the dolerite dykes in the Lala area yields a Sensitive High-Resolution Ion Microprobe (SHRIMP) zircon U-Pb age of 1710 ± 8 Ma (Guan et al., 2011).

The Kunyang Group is located in the central and northern parts of the Yunnan Province and is divided into the lower Kunyang Group (also known as the Dongchuan Group) comprised by the Yinmin, Luoxue, E'touchang, and Lvzhijiang formations. The Yinmin Formation consists of interbedded mafic volcanic breccia, intermediate to mafic banded tuff, volcaniclastic tuff and silicified keratophyre. Porphyritic monzogranite intruding the Yinmin Formation yields a LA-ICP-MS zircon U-Pb age of 1730 ± 15 Ma, and a dolerite dyke from the area has a LA-ICP-MS zircon U-Pb age of 1767 ± 15 Ma (Wang et al., 2013c; Guo et al., 2014a). The Luoxue Formation consists of greenish grey, greyish white, and red thick-layered algal dolomite, siliceous dolomite, and muddy sandy dolomite. The E'touchang Formation contains dark grey, dark green shale and minor amounts of shallow sandstone with lenses of dolomite, limestone and conglomerate. The Lvzhijiang Formation consists of dolomite and dolomitic limestone, with local slate and phyllite after shale.

The upper Kunyang Group includes the Huangcaoling (also known as the Dayingpan Formation), Heishantou, Dalongkou and Meidang formations. The Heishantou Formation comprises argillaceous and clastic sedimentary rocks, with argillaceous limestone, and mafic pyroclastic units. Tuff samples from the formation yield SHRIMP zircon U-Pb ages of 1032 ± 9 to 995 ± 15 Ma (Greentree et al., 2006; Zhang et al., 2007). The Dalongkou Formation is made up grey medium- to thick-bedded limestone and dolomitic limestone, with local marlstone, slate and phyllite (after shale), and siderite beds. The Meidang Formation consists of interbedded sandstone and shale, and minor pyroclastic rocks metamorphosed at greenschist facies.

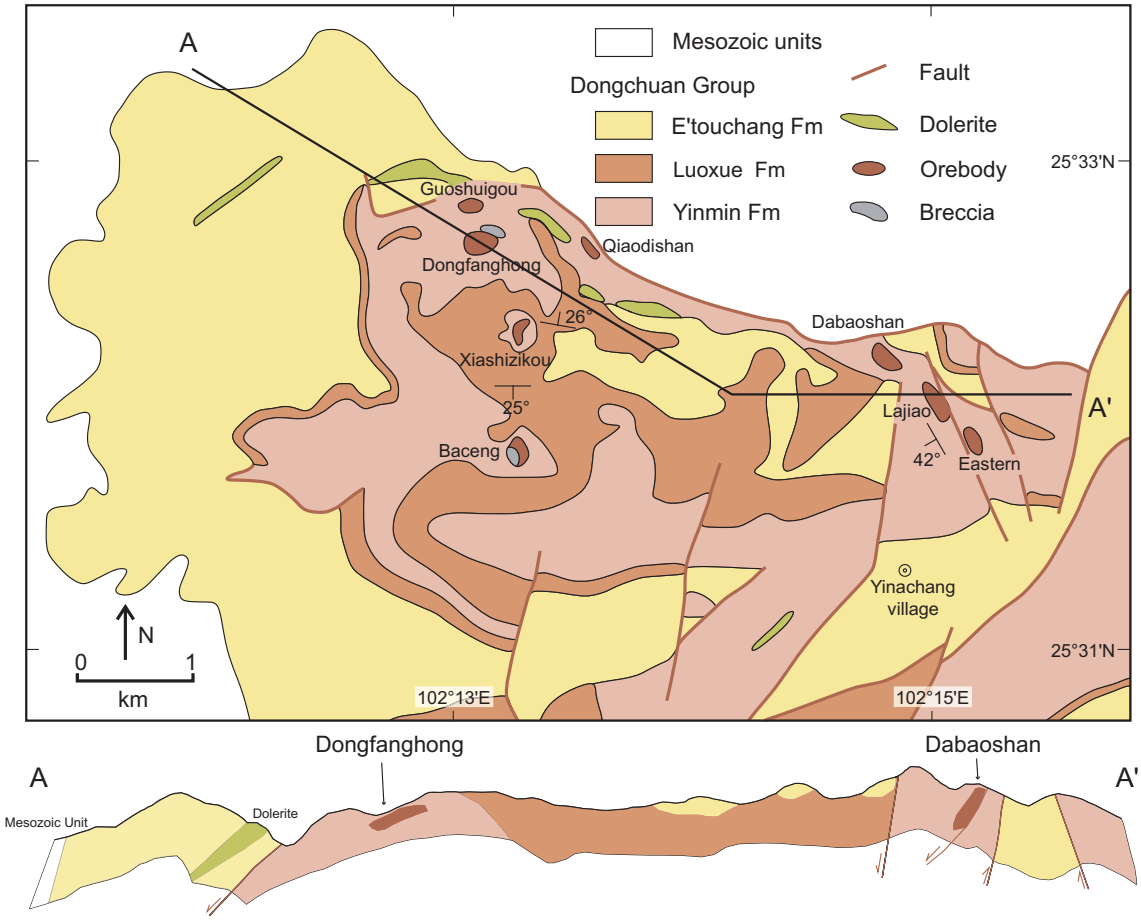


**Fig. 2.** Geological map of the mineralised Yinachang region and cross section A-A′ (after Li et al., 2015; Zhao et al., 2015).

**Table 2**
Ages published on the Yinachang deposit.

| No. | Sample-type | Dating method | Age (Ma) | ± | Interpreted significance | References |
|---|---|---|---|---|---|---|
| 1 | Biotite | K-Ar | 809 | 4 | Metamorphic age | Chen (1994) |
| 2 | Ore | Pb-Pb | 1037 | | Metamorphic age | Wu et al. (1998) |
| 3a | Quartz vein | $^{40}$Ar-$^{39}$Ar | 784 | 1 | Gangue age | Ye et al. (2004) |
| 3b | Quartz vein | $^{40}$Ar-$^{39}$Ar | 784 | 9 | Gangue age | Ye et al. (2004) |
| 4 | Banded ore | Sm-Nd | 1617 | 100 | Gangue age | Yang et al. (2005) |
| 5 | Fluorite | Sm-Nd | 1539 | 40 | Gangue age | Yang et al. (2005) |
| 6 | Tuff & volcanic breccia | U-Pb | 1750 | | Yinachang Formation | Ye et al. (2013) |
| 7 | Chalcopyrite | Re-Os | 1690 | 99 | Metallogenic age | Ye et al. (2013) |
| 8 | Magmatic breccia | U-Pb | 1739 | 13 | Magmatism age | Hou et al. (2013) |
| 9a | Mo, 1st generation | Re-Os | 1654 | 7 | Metallogenic age | Zhao et al. (2013a) |
| 9b | Mo, 2nd generation | Re-Os | 1451 | 6 | Metallogenic age | Zhao et al. (2013a) |
| 10 | Chalcopyrite | Re-Os | 1651 | 6 | Metallogenic age | Hou (2013) |
| 11 | Garnet | Sm-Nd | 901 | 57 | Metamorphic age | Hou (2013) |
| 12 | Biotite | $^{40}$Ar-$^{39}$Ar | 911 | 12 | Metamorphic age | Hou (2013) |
| 13 | Disseminated chalcopyrite | Pb-Pb | 1112 | 63 | Metamorphic age | Hou (2013) |
| 14 | Veined chalcopyrite | Pb-Pb | 881 | 41 | Metamorphic age | Hou (2013) |
| 15 | Dolerite | U-Pb | 1728 | 4 | Magmatism age | Guo et al. (2014a) |
| 16 | Biotite schist from wallrock | K-Ar | 789 | | Metamorphic age | Hou (2013) |
| 17 | Muscovite from wallrock | K-Ar | 827 | | Metamorphic age | Hou (2013) |

The Huili Group is a thick (> 10 km) and widespread metamorphosed sequence containing sandstone and shale, dolomitic carbonate, intermediate to mafic volcanic rocks, and black carbonate and marl. Its contact with the underlying crystalline rocks (orthogneiss and paragneiss) in the Precambrian Kangding Complex is unclear. The base of the group is intruded by mafic dykes yielding a LA-ICP-MS zircon U-Pb age of 1694 ± 16 Ma (Wang et al., 2013a).

### 2.2. Ore deposit geology

The Yinachang Fe-Cu-Au-U-REE deposit is located in a structurally complex area west of the Dajianshan Thrust and east of the Lvzhijiang Fault (Fig. 1b). The rocks in the area are greenschist facies conglomerate, hematite-bearing sandstone and shale, carbonaceous shale, muddy dolostone, dolostone, and locally present mafic and intermediate volcanic rocks of the Kunyang Group (Fig. 2).

The mineralised zone comprises eight lenticular orebodies forming a

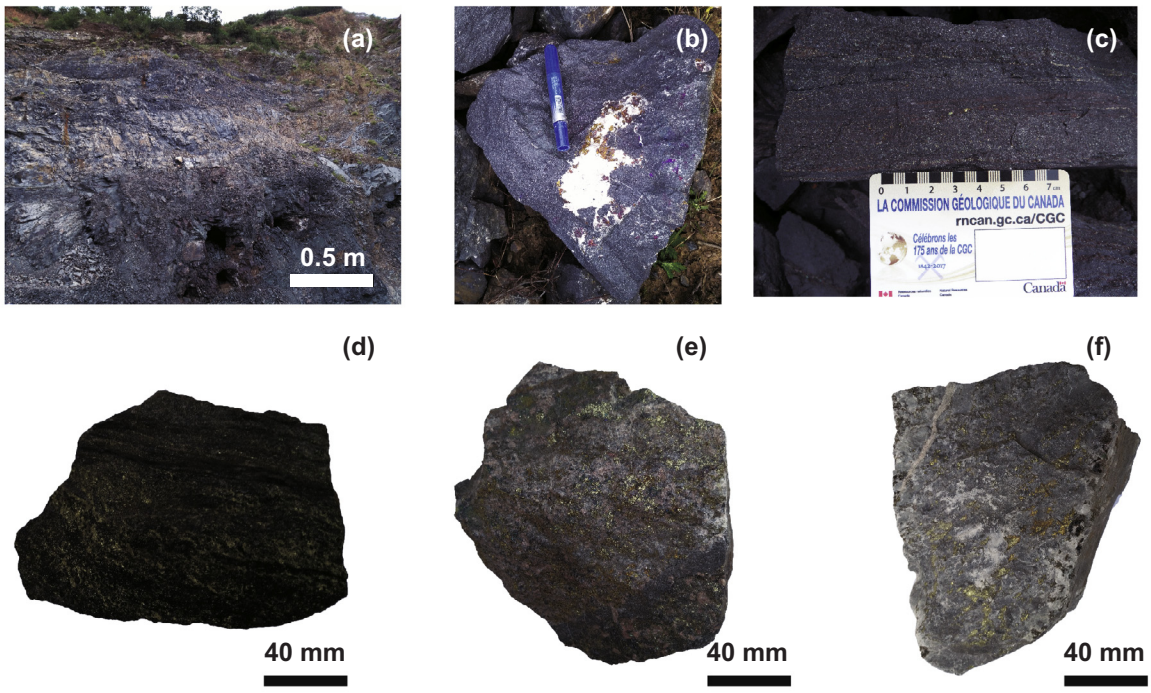


**Fig. 3.** Photographs: (a) stratiform orebody in contact with a carbonate unit; (b) massive ore in the Qiaodishan mine containing high-grade magnetite; (c) banded ore from the Dongfanghong mine; (d) banded ore from the Dongfanghong mine; (e) vein-type ore with high-grade chalcopyrite and REE minerals from the Guoshuigou mine; and (f) disseminated ore from the Qiaodishan mine.

4.5 km long and ~1.7 km wide, and includes the Dabaoshan, Lajiao and Eastern mines in the east and the Xiashizikou, Baceng, Dongfanghong, Guoshuigou and Qiaodishan mines in the west (Fig. 2; Table 2).

The combined resource of the mineralisation at Yinachang is 3.74 Mt averaging 45% Fe, 69,400 t averaging 1% Cu, and 12,800 t averaging 0.3% REE. Also present are 1360 t Nb, 700 t Co, and 1400 t Mo. The host rocks are magnetite-bearing dark greenschist (after basaltic units), biotite schist and sericitic schist, which commonly contain an early sodium alteration followed by magnetite-hematite, magnetite, polymetallic sulphides, sulphide veins, and late barren quartz veins. The mineralisation is banded in places resembling banded-iron formation (BIF).

The ore bodies are stratiform, lenticular, and often bifurcated, and containing magnetite, pyrite, hematite, chalcopyrite, bornite, and cobaltite including the gangue minerals quartz, calcite, dolomite, fluorspar, and biotite. The Fe-Cu deposits are interlayered with schist and slate derived from shale, dolomite, and silicified dolomitic schist and limestone (Fig. 3a). The selvages are altered at a metre-scale, characterised by the assemblage silica-biotite-sericite-siderite-garnet. The ore is massive and less commonly banded, disseminated, or veined. The massive ore contains magnetite with small amounts of other sulphides and apatite (Fig. 3b). The banded ore consists of magnetite, siderite, apatite, chalcopyrite, cobaltite, molybdenite, cassiterite, monazite, bastnaesite, parisite, and vandendriesscheite (Fig. 3c, d). Vein type ore contains variable proportions of magnetite rich in REEs, siderite, chalcopyrite, cobaltite, molybdenite and cassiterite, (Fig. 3e). The disseminated ore consists of chalcopyrite or magnetite in dolomite (Fig. 3f). Cobaltite and cassiterite rim chalcopyrite, chalcopyrite rims molybdenite, and chalcopyrite is partly replaced by vandendriesscheite (Fig. 4a–e). Apatite also contains high concentrations of REEs including monazite (Fig. 4d, f). The deposit is also characterised by a pre-ore Na-(Fe) alteration, and Fe(-REE) and Cu(-REE) mineralisation (Li et al., 2015).

## 3. Sampling and petrology

Diorite samples 16DFH-51 and 16DFH-54 were collected from the Dongfanghong mine (Group A) and gabbro samples 16QDS-61 and 16QDS-61-1 were collected from the Qiaodishan mine (Group B). The four samples were petrologically studied (Fig. 5). The diorite samples were collected from hydrothermally altered banded ore at the Dongfanghong mine, the gabbro samples are from the Yinmin Formation, and samples of the massive magnetite ore are from the Qiaodishan mine.

The diorite samples are medium-grained containing subhedral to euhedral plagioclase with sericite alteration (~65 wt%), amphibole (~22–27 wt%) altered to chlorite and calcite, biotite (~5–10 wt%) altered to chlorite, and irregular-shaped opaque minerals (~2–3 wt%). The plagioclase is altered to sericite and clay minerals.

The gabbro samples are coarse-grained containing subhedral to euhedral sericite-altered plagioclase (~45–50 wt%), hornblende (~45–50 wt%) with actinolite alteration, chlorite and opaque minerals, fine-grained quartz (~1–2 wt%), and scattered opaque minerals (~3–4 wt%).

## 4. Analytical methods

The rock samples were milled to a 200 mesh at the Hebei Regional Geological Survey Research Institute in Langfang, and sent to the Geophysical and Geochemical Exploration Institute of the Chinese Academy of Geological Sciences laboratory for whole-rock major and trace element analyses (Table 3; Supplementary Table 1).

Zircons were separated from the samples using conventional heavy liquids, magnetic separation techniques, and handpicking under a binocular microscope at the Langfang Geological Exploration Technology Services Limited. The zircon grains were mounted in epoxy, and then polished for subsequent cathodoluminescence (CL) examination and LA-ICP-MS analyses. The CL imaging was performed at the Electronic Microscope Laboratory of the School of Physics, Peking University. The

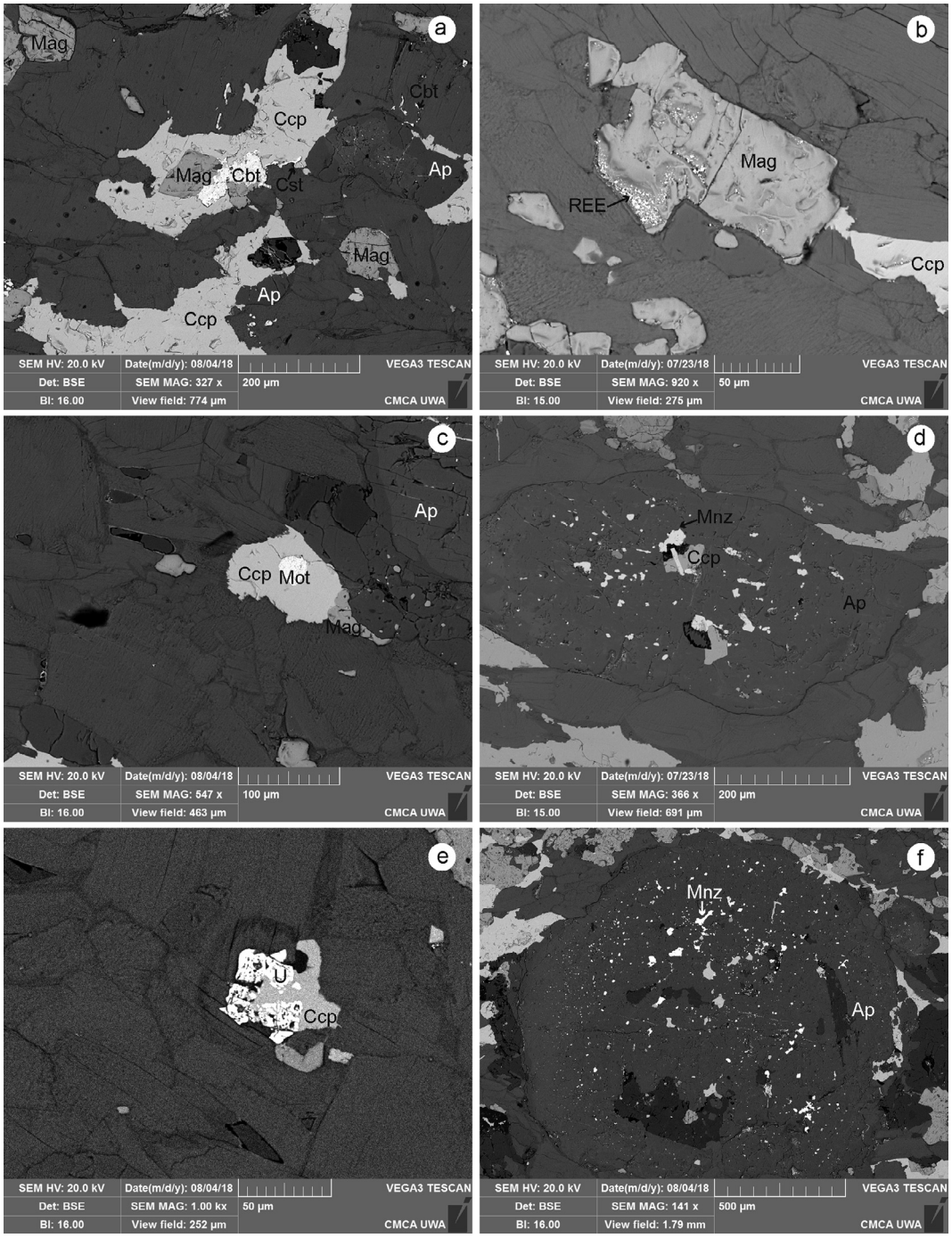


**Fig. 4.** Back Scattered Electron (BSE) images of different type of ore: (a) BSE image of banded ore showing a close association between magnetite, chalcopyrite, cobaltite, cassiterite and apatite; (b) BSE image showing the relationship between magnetite and the REE minerals bastnaesite and parasite distributed on the surface of magnetite; (c) BSE image showing molybdenite inclusions in chalcopyrite; (d) BSE image showing apatite with inclusions of monazite crosscutting chalcopyrite; (e) BSE image showing vandendriesscheite ($Pb_{1.6}(UO_2)_{10}O_6(OH)_{11}{\cdot}11H_2O$) overprinting chalcopyrite; and (f) BSE image showing apatite peppered with inclusions of monazite. Abbreviations: Ap = Apatite, Cbt = Cobaltite, Ccp = Chalcopyrite, Cst = Cassiterite, Mag = Magnetite, Mnz = Monazite, Mot = Molybdenite, REE = Rare Earth Element mineral.

zircons were analysed for U-Pb isotopes and in-situ trace element concentrations using a LA-ICP-MS ion microprobe, with a spot size of 36 µm, at the State Key Laboratory of Geological Processes and Mineral Resources of China University of Geosciences (Beijing). The LA-ICP-MS consists of a 7500-plasma mass spectrometer and UP193-SS laser ablation manufactured by the American Agilent and American New Wave companies, and helium was used as the carrier gas of the denudation material. The laser frequency was set at 10 Hz with a laser wavelength of 193 nm, a beam spot diametre of 36 µm, laser pre-denudation time set as 5 s, and denudation time set as 45 s. The 91500-zircon standard was used as an external standard, the international NIST610-glass standard for trace elements was used as an internal standard. The measured Pb/U isotopic ratios in unknown zircons were corrected using the 417 Ma TEM-zircon standard every fourth or fifth analysis. The common Pb component was estimated from $^{204}Pb$ counts using the method of Andersen (2002), and the data were processed using the special software Glitter 4.4. The age calculations and plotting of concordia diagrams were completed using the ISOPLOT 3.7 software of

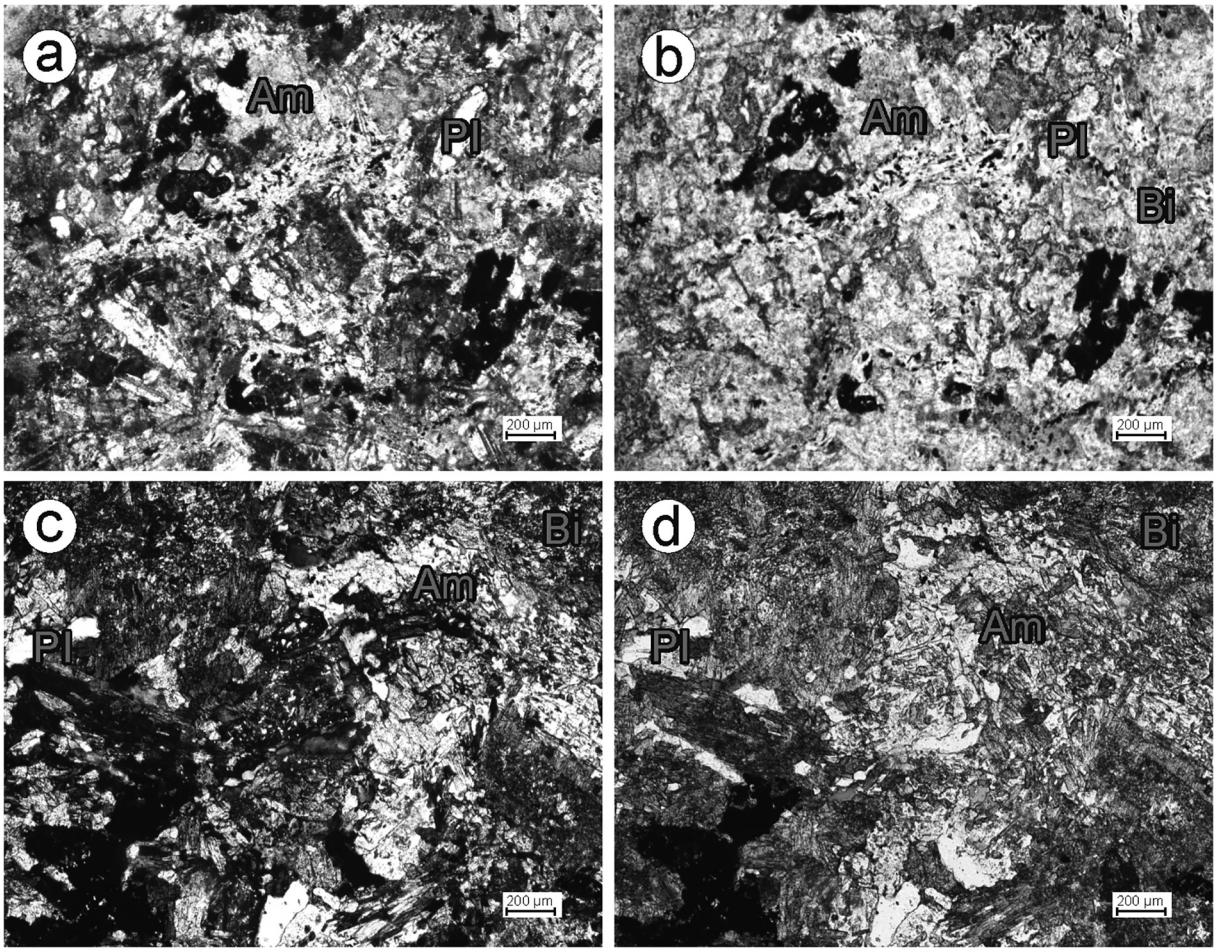


**Fig. 5.** Photomicrographs showing the mineral textures of the diorite (a, b) and gabbro (c, d) samples from the Yinachang deposit: (a) under crossed polarized light; (b) under plane-polarized light; (c) under crossed polarized light; and (d) under plane-polarized light. Abbreviations: Pl-plagioclase, Am-amphibole, Bi-biotite.

**Table 3**
Whole-rock major and trace element analytical methods.

| Elements | Analytical method |
|---|---|
| Ag, Bi, Cd, Co, Cs, Cu, Hf, Mo, Nb, Ni, Pb, Sb, Sc, Ta, Th, U, W, Zn, Ce, Dy, Er, Eu, Gd, Ho, La, Lu, Nd, Pr, Sm, Tb, Tm, Y & Yb | Plasma mass spectrometry (ICP-MS) |
| As | Hydride-atomic fluorescence spectrometry (HG-AFS) |
| Ba, Rb, S, Sr, V, Zr, Cr & Ga | X-ray fluorescence spectrometry (XRF). |
| Be & Li | Plasma spectroscopy (ICP-OES) |
| Se | Hydride-atomic fluorescence spectrometry (HG-AFS) |
| Sn | Emission spectrometry (ES) |
| Hg | Cold vapour-atomic fluorescence spectrometry (CV-AFS) |
| $SiO_2$, $Al_2O_3$, MgO, MnO, $TiO_2$, $Fe_2O_{3T}$, $P_2O_5$, $K_2O$, CaO & $Na_2O$ | X-ray-fluorescence spectrometry (XRF) |
| $Fe_2O_3$ | X-ray-fluorescence spectrometry (XRF) & Volumetric method (VOL) |
| FeO | Volumetric method (VOL) |
| LOI | Gravimetric method |
| Au | Flameless atomic absorption spectrometry (AAN) & Flame atomic absorption spectrometry (AAS) |

Ludwig (2008). The zircon U-Pb isotope data are presented in Supplementary Table 2.

## 5. Results

### 5.1. Geochemical characteristics

All the major element compositions were normalised to 100% in a volatile-free basis during this study. The two mafic igneous samples from the Yinachang deposit plot in the gabbro to monzogabbro (gabbroic) fields and the two intermediate samples plot in the gabbroic diorite to diorite (dioritic) fields in the total alkali vs silica (TAS) diagram for volcanic rocks (Fig. 6a). The diorite samples also plot in the shoshonite series field in Fig. 6b, the shoshonitic to ultrapotassic field in Fig. 6c and the calc-alkaline field in Fig. 6d. The gabbro samples plot in the high-K calc-alkaline field in Fig. 6b, the calc-alkaline field in Fig. 6c and tholeiitic field in Fig. 6d.

The diorite samples are characterised by high $Al_2O_3$ (17.29–18.87 wt%) and low $TiO_2$ (average of 0.71 wt%) assays that are characteristic of shoshonitic rocks. The gabbro samples have high $Al_2O_3$ (12.96–13.60 wt%), high $FeO_T$ (18.11–18.15 wt%) assays, and low $TiO_2$ (2.79–3.01 wt%) assays (typical of calc-alkaline series).

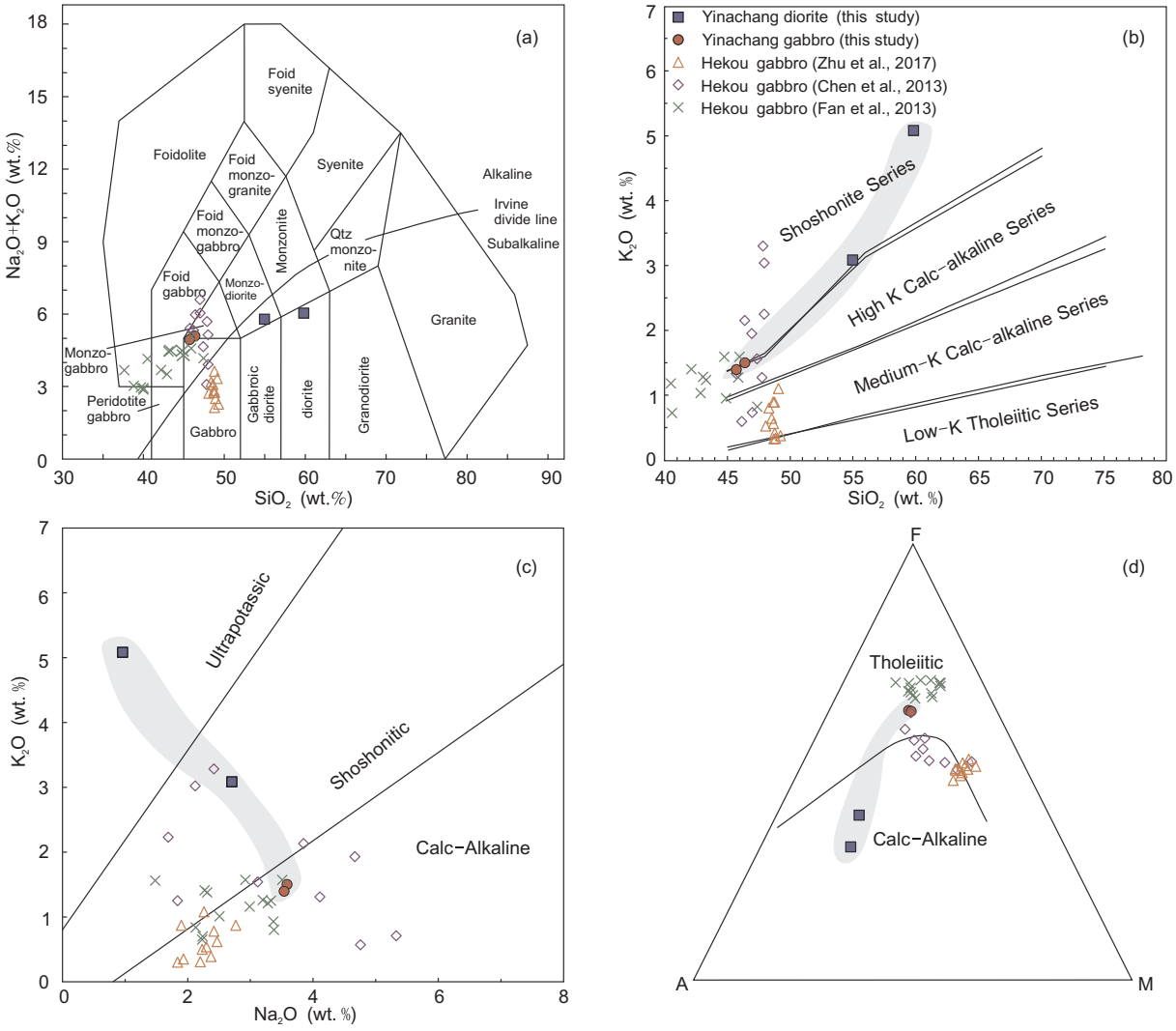


**Fig. 6.** Diagrams: (a) TAS ($Na_2O + K_2O$ vs $SiO_2$) plot (after Middlemost, 1994) showing that the samples collected for this study are dioritic (diorite and monzodiorite), and gabbroic (gabbro to monzogabbro) in composition; (b) $K_2O$ vs $SiO_2$ plot (after Peccerillo and Taylor, 1976; Middlemost, 1985); (c) $K_2O$ vs $Na_2O$ (after Middlemost, 1972); (d) A ($Na_2O + K_2O$) – F ($FeO + 0.8998 \times Fe_2O_3$) – M (MgO) plot (after Irvine and Barager, 1971). Data from Chen et al. (2013), Fan et al. (2013), Zhu et al. (2017), and this study.

The primitive-mantle normalised trace elements for the diorite and gabbro are relatively enriched in large-ion lithophile elements (LILEs), Rb and U compared to the other samples (except for the Hekou gabbro in Fig. 7g), and are strongly depleted in the high-field-strength element (HFSE) Sr (Fig. 7a). The depletion in $Sr^{2+}$ is indicative of plagioclase fractionation from the parental magma, and Rb, being a highly incompatible element, would have concentrated in the parental magma and eventually substituting for $Ca^{2+}$ in minerals such as plagioclase (Na-$CaAlSi_3O_8$).

The ΣREE contents of the dioritic samples assay 125–248 ppm. The REE distribution diagram shown in Fig. 7b shows that the diorite is moderately enriched in LREEs and has a relatively flat HREE pattern. The LREE/HREE ratio for the diorite is 10.2–16.98, the $(La/Yb)_N$ ratio is 11.81–30.83, the δCe value is 0.94–0.97, and Eu has a positive anomaly with δEu values of 0.94–1.47.

Fig. 7b shows that the gabbro samples from this study are slightly enriched in LREEs, and have slightly negative Eu anomalies and relatively flat HREE patterns as compared to the dioritic samples. The ΣREE content is 193–203 ppm, the LREE/HREE ratio is 2.86–2.88, $(La/Yb)_N$ is 2.24–2.33, δCe is 0.98–1.07, and δEu is 0.83–0.86. The slight negative Eu anomaly indicates that plagioclase was not significantly fractionated from the gabbro's magma source. The gabbro's REE pattern resembles that of an enriched mid-ocean ridge basalt (EMORB; Fig. 7j).

The geochemistry of the intermediate and mafic igneous rocks elsewhere in the Kangdian region have been collected from the literature for comparison with our samples (Chen et al., 2013; Fan et al., 2013; Zhu et al., 2017). Fig. 6b–d shows that the Hekou gabbro plots in the high K calc-alkaline field (Chen et al., 2013; Fan et al., 2013). The Yinachang diorite in Fig. 7b and Hekou gabbro in Fig. 7(f, h) have normalised REE patterns that dip steeply to the right, which is consistent with an OIB tectonic setting (c.f. Fig. 7j). The Yinachang gabbro also has a normalised REE pattern like those of the Hekou gabbro in Fig. 7d (except for the slight Eu anomaly in the Hekou gabbro). The overall pattern of these samples are indicative of an E-MORB tectonic setting (c.f. Fig. 7j).

### 5.2. LA-ICP-MS zircon U-Pb dating

Twenty zircon grains from the Yinachang diorite were LA-ICP-MS U-Pb dated. Most of the zircons are euhedral or subhedral with lengths of 50–150 μm and widths of 30–70 μm. The CL images and the analysed spots of zircons are shown in Fig. 8. The zircons have obvious oscillatory zoning typical of a magmatic source and some have discordant cores enclosed with younger rims.

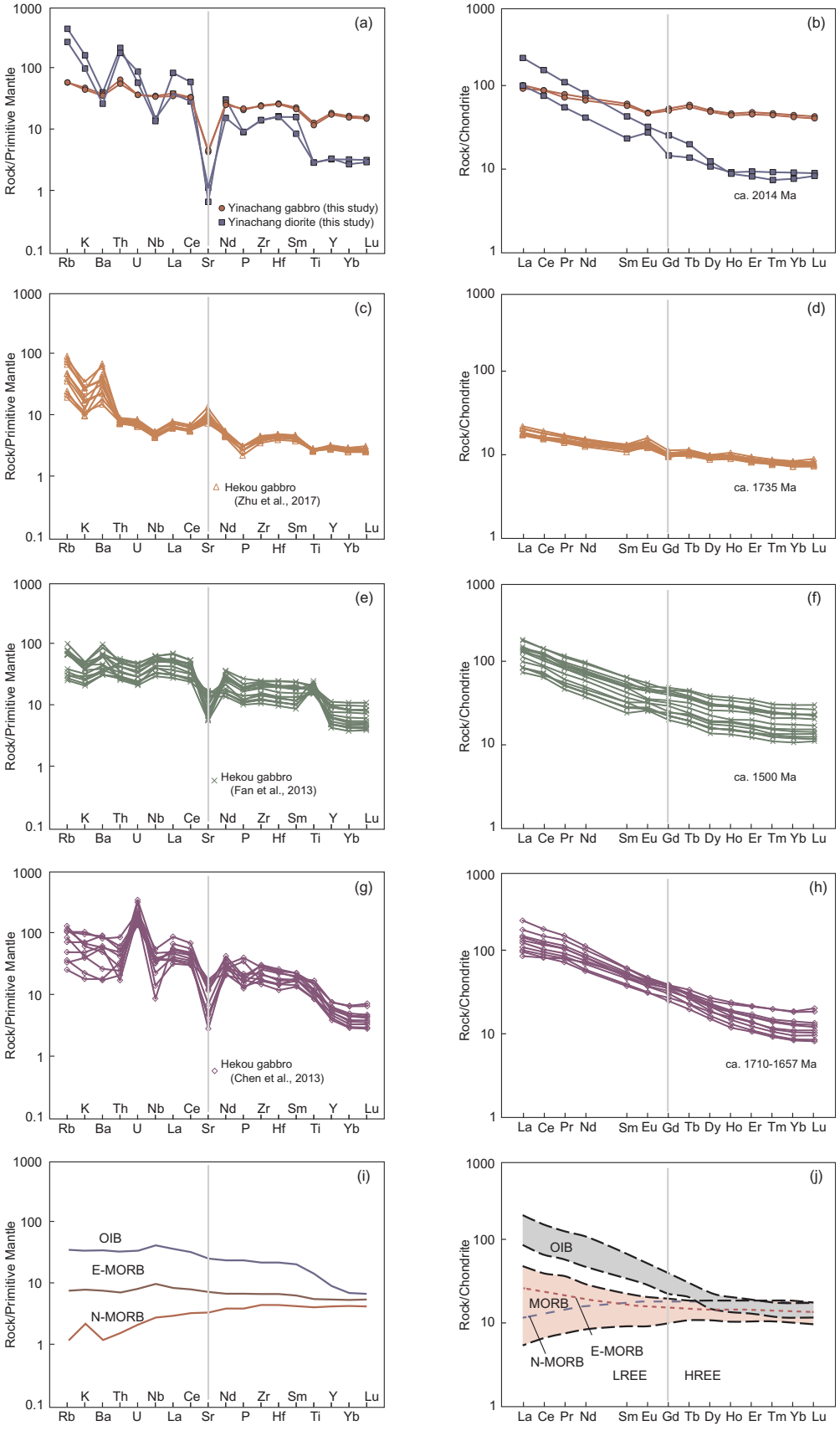


**Fig. 7.** Normalised diagrams showing: (a) Primitive Mantle normalised trace element plot of the Yinachang diorite and gabbro (this study); (b) Chondrite normalised REE plot of the Yinachang diorite and gabbro (this study); (c) Primitive Mantle normalised trace element plot of the Hekou gabbro (from Zhu et al., 2017); (d) Chondrite normalised REE plot of the Hekou gabbro (from Zhu et al., 2017); (e) Primitive Mantle normalised trace element plot of the Hekou gabbro (from Fan et al., 2013); (f) Chondrite normalised REE plot of the Hekou gabbro (from Fan et al., 2013); (g) Primitive Mantle normalised trace element plot of the Hekou gabbro (from Chen et al., 2013); (h) Chondrite normalised REE plot of the Hekou gabbro (from Chen et al., 2013); (i) examples of Primitive Mantle normalised plots of MORB- and OIB-type basalts (Sun and McDonough, 1989); and (j) examples of Chondrite normalised REE plots of MORB- and OIB-type basaltic rocks from the Tethyan Suture in western Turkey (Aldanmaz et al., 2008). Primitive Mantle normalising values and Chondrite normalising values are from Sun and McDonough (1989).

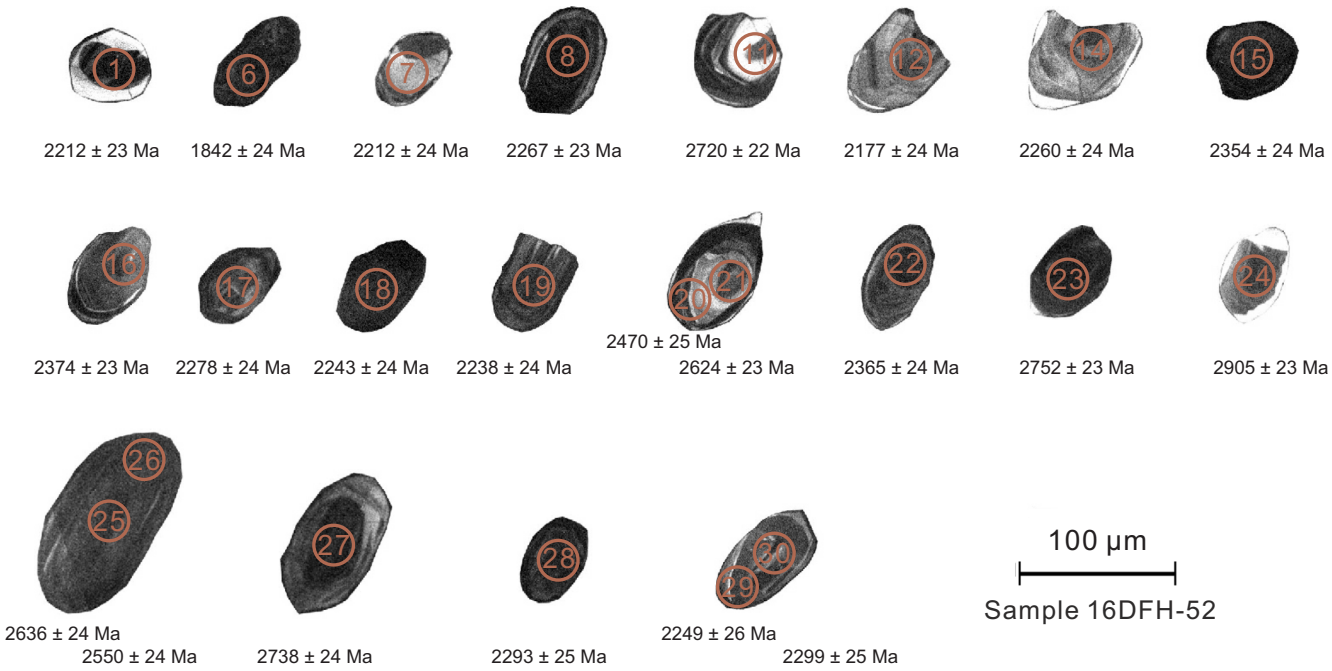


**Fig. 8.** Cathodoluminescence (CL) image of representative zircons in the diorite samples from the Yinachang deposit.

Zircons from the Yinachang diorite assay 128–765 ppm U and 38–1317 ppm Th with Th/U ratios of 0.25–3.12, which are also characteristic of a magmatic origin. The Th/U ratios of Spots 8, 11, 15, 18, 19, 23, 24, 29 and 30 are < 1 (indicative of a xenocrystic origin). The concordia plots in Fig. 9 show the zircons have experienced an open-system alteration with lose in $^{207}Pb$ and $^{206}Pb$ in equal amounts forming a straight line between an upper intercept (representing the age of the zircons) and a lower poorly dated intercept representing a metamorphic event. The plot shows at least two distinct zircon populations are present with upper intercept dates of 2629 ± 64 and 2014 ± 30 Ma, and imprecise lower intercepts of 906 ± 100 Ma for the zircon cores, and 191 ± 110 Ma for the rim (Fig. 9).

Zircons from the gabbro are short and columnar in size with lengths of 80–180 μm and widths of 40–60 μm. The zircons have LA-ICP-MS assays of 1742–6877 ppm U, 3469–38748 ppm Th and have Th/U ratios of 0.77–9.51, which are indicative of a magmatic origin. The high U contact content of these zircons has resulted in the destruction of their crystal structure making them metamict. This is expressed by their black CL images and inaccurate LA-ICP-MS U-Pb dates with error estimates reaching almost 393 Ma (Fig. 10). The dates determined from the gabbro have thus been rejected.

### 5.3. Zircon trace elements chemistry analyses

Twenty zircons from the diorite and 25 zircons from the gabbro samples were analysed with a LA-ICP-MS for their trace element geochemistry (Supplementary Tables 3 and 4), and their Chondrite-normalised REE patterns are presented in Fig. 11.

The ΣREE for the diorite is between 337 and 1958 ppm, LREE/HREE ratios are between 0.04 and 0.39, $(La/Yb)_N$ ratios are between 0.0004 and 0.1312 (relating to a loss in LREEs and enrichment in HREEs with an anomalous δCe range of 0.96 to 10.25), and a depleted δEu range of 0.65 to 2.62. The ΣREE for the gabbro ranges between 35,237 and 10,604 ppm, the LREE/HREE ratio is 0.08–0.81, and the $(La/Yb)_N$ values is between 0.01 and 0.15. These data correspond to a loss in LREEs and enrichment in HREEs. The δCe ranges from 1.14 to 2.61 corresponding to a moderately positive Ce anomaly, and the δEu value ranges from 0.35 to 1.27 corresponding to a moderately negative Eu anomaly.

#### 5.3.1. Zircon saturation temperature and Ti content temperature

Zircon Ti thermometer is a geochemical routine for estimating zircon crystallisation temperatures (Watson and Harrison, 2005; Watson et al., 2006; Ferry and Watson, 2007). The addition of Ti into zircon crystals is controlled by the temperature and activity of $TiO_2$ ($a_{TiO2}$). Ferry and Watson (2007) combined the results of high-temperature and high-pressure experiments with zircon analyses, and calculated a linear equation using the proportion of Ti in zircons:

$$T_{(\text{Zircon Ti temperature °C})} = \left\{\frac{4800 \pm 86}{((5.711 \pm 0.072) - \log(ppm\ Ti\ in\ zircon))}\right\} - 273.15,$$

where the activity of $SiO_2$ and $TiO_2$ in the magma is taken to be 1.

Using the formula above, the diorite's zircon crystallisation temperature is 703–1022 °C and the gabbro's zircon crystallisation temperature is 904–1862 °C (Supplementary Tables 3 and 4). However, the estimated temperature range for zircons from the gabbro is too widely spread for a meaningful interpretation.

Another method for estimating the temperature that zircons crystallise is presented by Watson and Harrison (1983), who experimented on the solubility of zircon at temperatures between 700 and 1300 °C, which are expected in a granitic magma. The distribution coefficient of a magma, which includes solid and liquid, is a function of temperature. Assuming that its activity coefficient is 1, the zircon saturation temperature is determined using the Zr solubility formula:

$$\text{Ln } D^{\text{Zr,Zrmelt}} = \left[-3.8 - 0.85 \times M - 1 + \frac{12900}{T}\text{°C}\right]$$

where DZr,Zrmelt is the ratio of Zr concentration (ppm) in zircon to that in the saturated melt, $M$ is the cation ratio (Na + K + 2Ca)/(Al···Si) in the granitic host. Rearranging the equation to yield $T$ results in a geothermometer for melt:

$$T_{Zr}(°C) = \left\{\frac{12900}{[Ln(496000/Zr_{melt}) + 0.85 \times M + 2.95]}\right\} - 273.15.$$

The Zr and Hf elements have very similar chemical characteristics, and assuming there is a negligible level of Hf in zircons, the proportion of Zr in a zircon ($ZrSiO_4$) is 49.6%, and the proportion of Zr in the

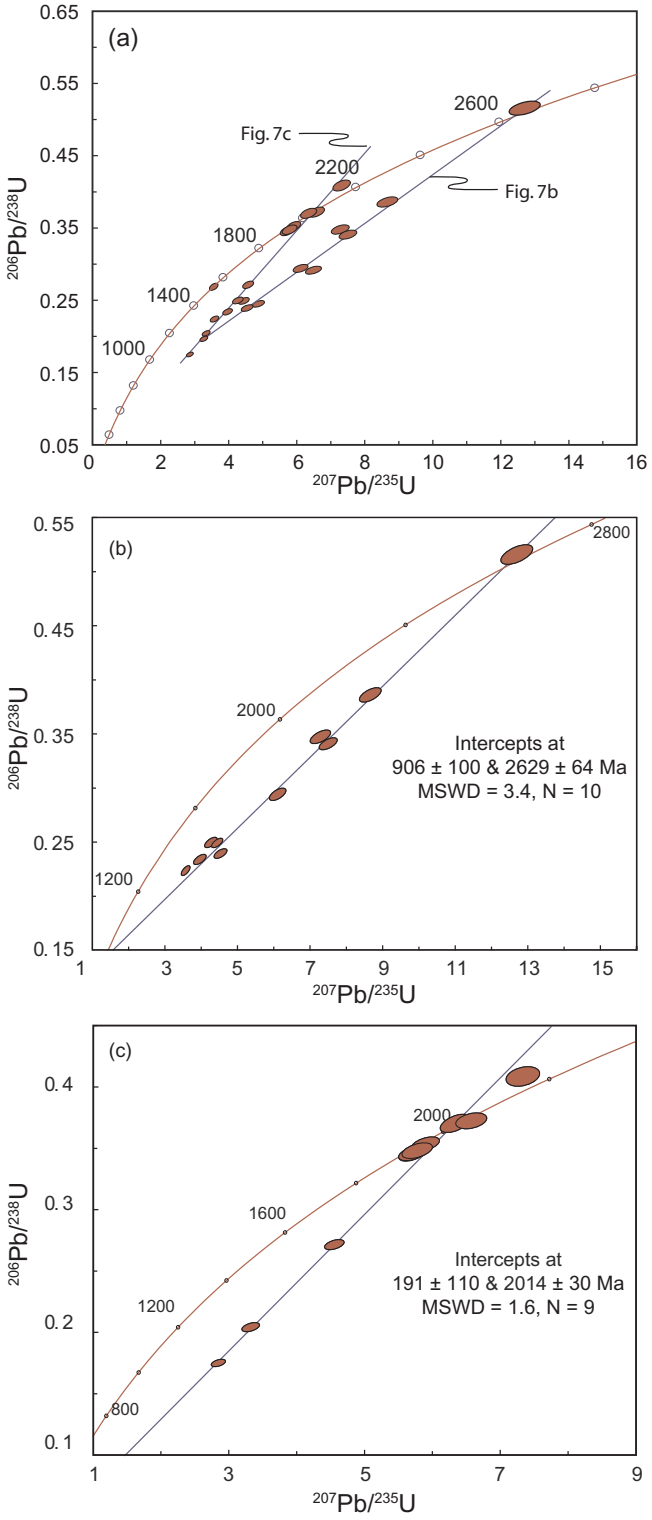


**Fig. 9.** U-Pb isotopic concordia plots of zircons from diorite at the Yinachang deposit.

whole-rock can be assumed to be the content of Zr in the parental magma (Watson and Harrison, 1983; Miller et al., 2003; Watson et al., 2006). Using the formula above, the zircon saturation temperatures for the Yinachang diorite vary between 765° and 808 °C, and those for the Yinachang gabbro vary between 694° and 706 °C, but these ranges are here regarded as being tentative.

*5.3.2. Crystallisation environment of magma*

Zircons are resistant to changes in temperature and can be stable at temperatures reaching ~1690 °C. This durability of zircons and their incorporation of cations such as REE, U, Th, Hf, Pb and Ti makes them records of the geochemical signature of the magma from which they crystallise (Cherniak et al. 1997a,b; Cherniak and Watson, 2001, 2007). In addition, oscillatory or sector zoning in magmatic zircons can provide evidence for the evolution of a magma. Magmatic and hydrothermal zircons can also be distinguished from each other by their $(Sm/La)_N$ versus La and δ(Ce) versus $(Sm/La)_N$ plots (Hoskin, 2005). Fig. 12 indicates that the zircons from the diorite are magmatic and hydrothermal and those from the gabbro are hydrothermal.

Trace elements such as U, Yb and Y in zircons can be used in U vs Yb and U/Yb vs Y discrimination diagrams to indicate whether their parental magma was emplaced in an oceanic or continental crust (Grimes et al., 2007). The zircons from the dioritic rocks plot in the continental field and those from the gabbro plot in the oceanic to continental crust fields (Fig. 13a, b). However, given that the zircons from the gabbro are metamict due to their enrichment in U, and the temperature estimated for the gabbro samples probably corresponds to the temperature of a hydrothermal event, this proposal must be regarded as tentative.

## 6. Discussion

### *6.1. Significance of geochronology for the origin of magmas*

The Palaeoproterozoic (ca. 2100–1800 Ma) Columbia Supercontinent has been reconstructed on geological and paleomagnetic grounds (c.f. Rogers and Santosh, 2002; Zhao et al., 2002; Joseph and Santosh, 2017). Fragmentation of this supercontinent began in the Mesoproterozoic along rift zones along the western margin of Laurentia, southern margin of Baltica, southeastern margin of Siberia, northwestern margin of South Africa, and northern margin of China (Zhao et al., 2002). The event is associated with widespread magmatism that continued until the emplacement of ca. 1270–1240 Ma dyke swarms leading to the final breakup of the supercontinent (Zhao et al., 2004).

The oldest rocks in the Yangtze Block are the Archaean (ca. 3300–2900 Ma) Kongling and Early Palaeoproterozoic (ca. 2400 Ma) Houhe complexes exposed in the northern part of the region (Gao et al., 1999; Qiu et al., 2000; Zhang et al., 2006). The region includes ca. 1850 Ma granites interpreted to represent an extensional tectonic event following a collisional event (Peng et al., 2009, 2012). Also present is the ca. 1730 Ma Haizi Granite emplaced during rifting along the western margin of the Yangtze Block (Wang et al., 2013c).

Zhao and Zhou (2011) and Zhao et al. (2013b) propose that the Kangdian region was situated in a Palaeoproterozoic intraplate-rift based on their interpretation of U-Pb geochronology and Hf isotopes systematics on detrital zircons from the Dongchuan Group. They also compared similar types of deposits located in the region and propose that IOCG deposits in the areas may be products of Columbia Supercontinental cycles (i.e. amalgamation and subsequent breakup). Wang et al. (2013b) interpret the gabbro in the Huili area at the western margin of the Yangtze Block as being derived from the Mantle and emplaced along faults in an extensional tectonic setting within the supercontinent.

Fan et al. (2013) propose that the ca. 1500 Ma magmatism in the Kangdian region is globally synchronous with Mesoproterozoic orogenic events and post-orogenic magmatism throughout Precambrian terranes. Furthermore, the ca. 1600–1200 Ma magmatism is believed to be related to mantle plumes affecting the Columbia Supercontinent (Rogers and Santosh, 2002; Zhao et al., 2002, 2004; Peng, et al., 2009; Evans and Mitchell, 2011; Silveira, et al., 2012).

Magmatism in the Kangdian region is Late Palaeoproterozoic (ca. 1800–1600 Ma) in age (Greentree and Li, 2008; Zhao et al., 2010; Zhao and Zhou, 2011; Zhu et al., 2011; Guan et al., 2011; Zhou et al., 2011;

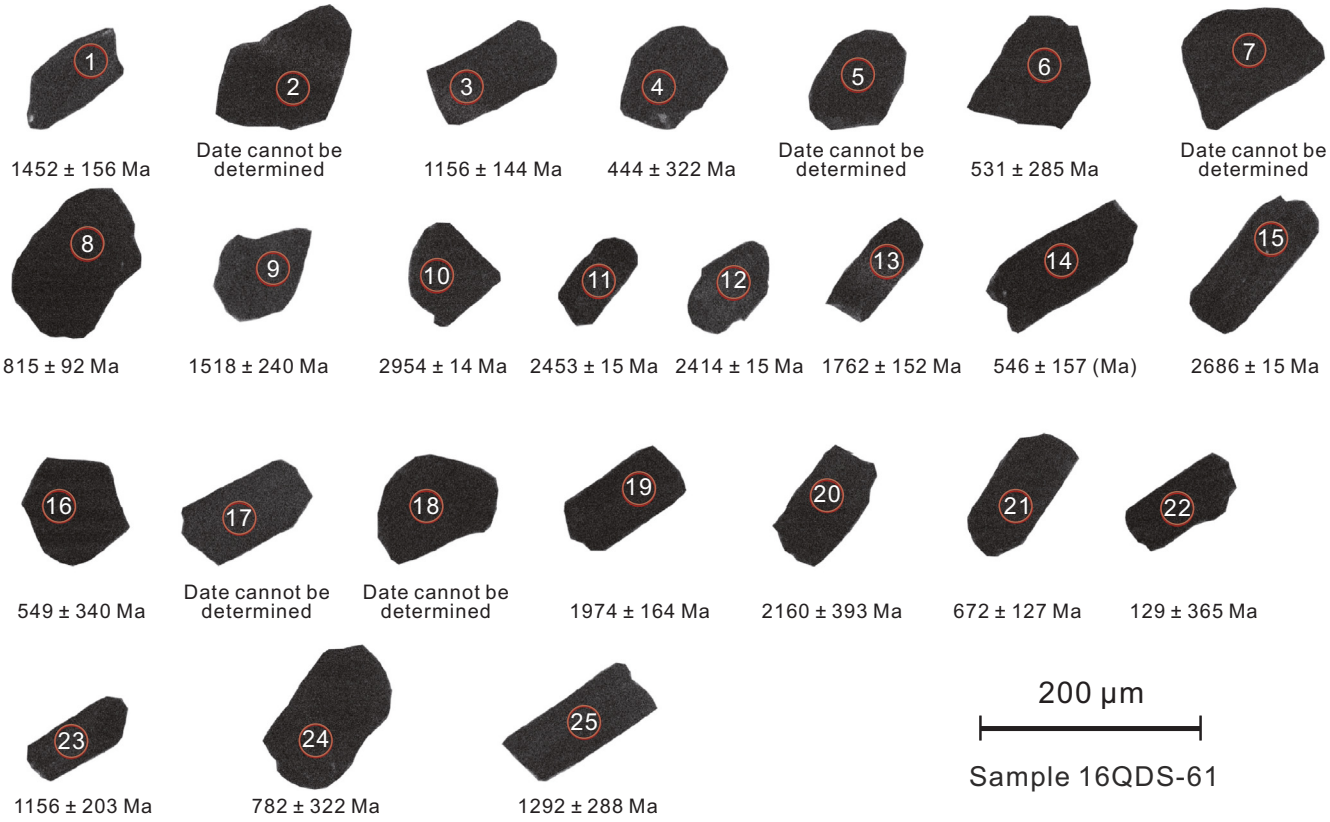


**Fig. 10.** Cathodoluminescence (CL) image of representative zircons from the gabbro at the Yinachang deposit.

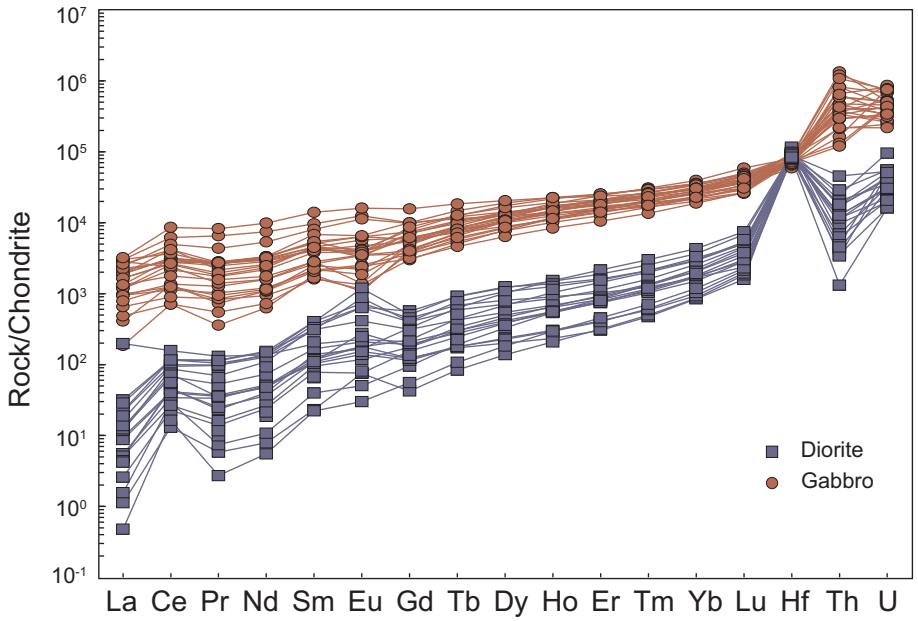


**Fig. 11.** Chondrite-normalised trace element geochemistry patterns of zircons in diorite and gabbro from the Yinachang deposit. All data are normalised to Chondrite values (after Sun and McDonough, 1989).

Wang et al., 2013a,b; Guo et al., 2014b). Both the combined zircon cores with the 2629 ± 64 dates and rims with the 2014 ± 30 Ma dates from the diorite shown in Fig. 9 are possibly xenocrystic. In this scenario, the zircon rims would representing a previously unrecognised Palaeoproterozoic metamorphism. These dates also indicate that the crust in the region includes Neoarchaean and Palaeoproterozoic substrates. Furthermore, the plots in Fig. 9 include imprecise lower intercepts at 906 ± 100 Ma for the zircon cores, and 191 ± 110 Ma for the rim. Even though these dates are only approximate, the ca. 906 Ma date coincides with the amalgamation of the Yangtze and Cathaysia blocks during ca. 900–800 Ma and probably records an Early Neoproterozoic metamorphic event (c.f. Wang et al., 2006; Li et al., 2007).

Ye et al. (2013) report a Re-Os date of ca. 1690 Ma for chalcopyrite at the Yinachang Fe-Cu-Au-U-REE deposit, which they interpret as the approximate age of the mineralisation that is slightly younger that the ca. 1735 Ma Hekou gabbro dated by Zhu et al. (2017), which is

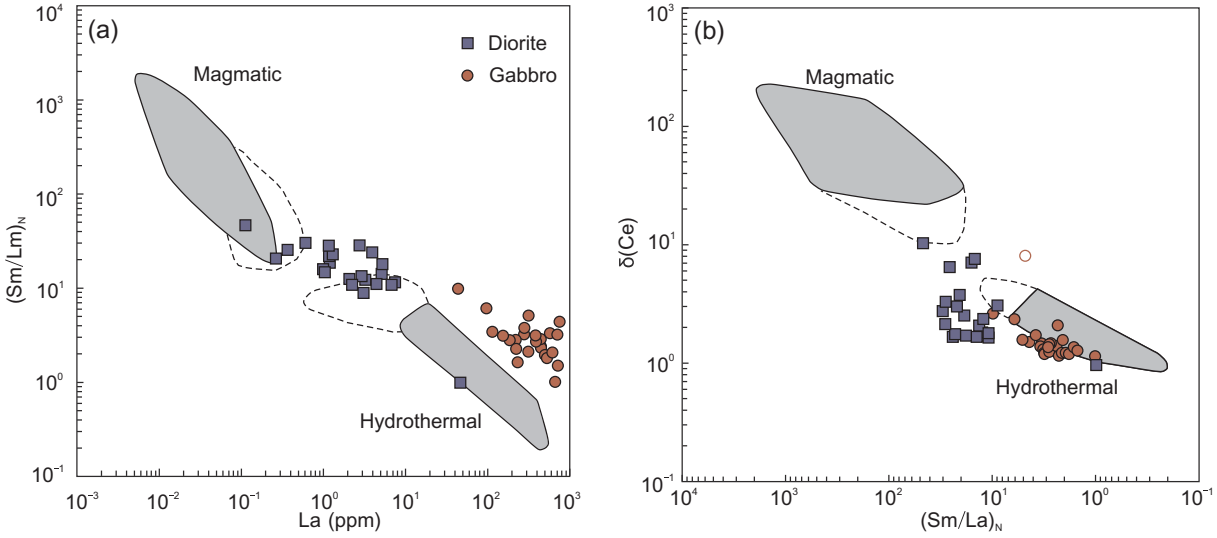


**Fig. 12.** Discrimination plots for magmatic and hydrothermal zircon: (a) Chondrite-normalised $(Sm/La)_N$ ratio vs La (ppm); and (b) Ce anomaly $(Ce/Ce^*)$ vs $(Sm/La)_N$ (after Hoskin, 2005).

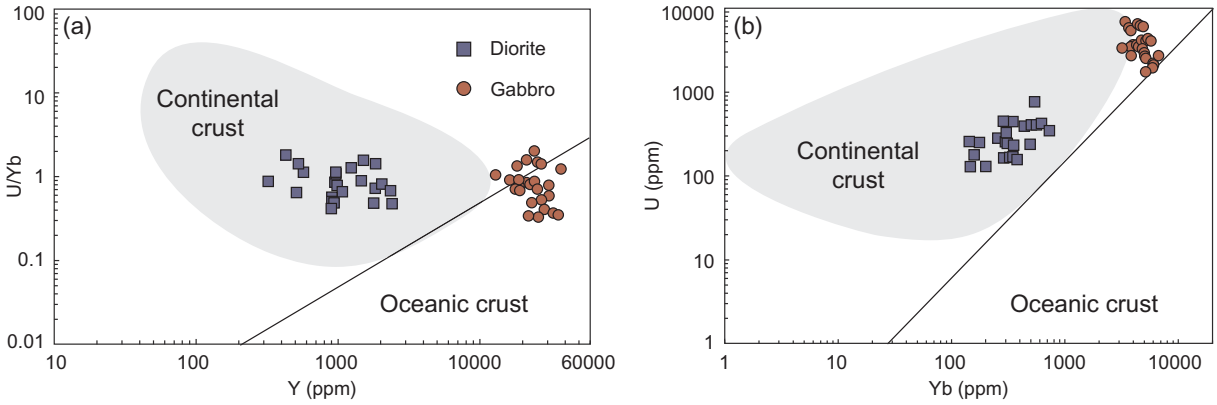


**Fig. 13.** Geochemical discriminant diagrams for zircon showing: (a) U/Yb vs Y; and (b) U vs Yb (after Grimes et al., 2007).

**Table 4**
Comparison of parameters between the magmatic rocks in the Kangdian region and the main geological end-members.

| Rock-types | Zr/Nb | La/Nb | Ba/Nb | Th/Nb | Th/La | Ba/La | Reference |
|---|---|---|---|---|---|---|---|
| Primordial Mantle | 14.8 | 0.94 | 9 | 0.1 | 0.1 | 9.6 | Weaver (1991) |
| N-MORB | 30 | 1.07 | 4.3 | 0.1 | 0.1 | 4 | Weaver (1991) |
| Continental Crust | 16.2 | 2.2 | 54 | 0.4 | 0.2 | 25 | Weaver (1991) |
| HIMU OIB | 2.7–5.5 | 0.6–0.8 | 4.7–6.9 | 0.1 | 0.1–0.2 | 6.2–9.3 | Weaver (1991) |
| EM I OIB | 3.5–13.1 | 0.8–1.3 | 9.1–23.4 | 0.1 | 0.1–0.2 | 11.3–19.1 | Weaver (1991) |
| EM II OIB | 4.4–7.8 | 0.8–1.2 | 6.4–13.3 | 0.1–0.2 | 0.1–0.2 | 7.3–13.5 | Weaver (1991) |
| Huili gabbro | 10.9–12 | 1.1–1.2 | 40.46–100 | 0.1 | 0.1 | 33.8–87.8 | Wang et al. (2013a) |
| Average | 11.3 | 1.1 | 62.82 | 0.1 | 0.1 | 55.4 | Wang et al. (2013a) |
| Dongchuang dolerite | 5.8–13.2 | 1–2.6 | 12.1–67.5 | 0.1–0.2 | 0–0.1 | 10.9–38.2 | Wang et al. (2013b) |
| Average | 10 | 1.5 | 33.15 | 0.1 | 0.1 | 22 | Wang et al. (2013b) |
| Dahongshan mafic granulite | 6–18.8 | 0.7–1.5 | 0.9–22.1 | 0.1–0.3 | 0.1–0.2 | 0.7–19.2 | Yang et al. (2004) |
| Average | 11.2 | 1.2 | 7.48 | 0.1 | 0.1 | 7.2 | Yang et al. (2004) |
| Hekou gabbro | 8.51–55.01 | 1.01–7.41 | 3.73–99.69 | 0.05–0.84 | 0.06–0.14 | 3.71–16.63 | Chen et al. (2013) |
| Average | 14.84 | 2.01 | 22.93 | 0.21 | 0.10 | 11.00 | Chen et al. (2013) |
| Hekou gabbro | 5.62–6.51 | 0.73–1.08 | 6.19–20.73 | 0.08–0.11 | 0.10–0.13 | 6.19–23.05 | Fan et al. (2013) |
| Average | 5.89 | 0.92 | 11.24 | 0.10 | 0.11 | 12.49 | Fan et al. (2013) |
| Hekou gabbro | 12.81–13.82 | 1.27–1.42 | 31.41–118.78 | 0.19–0.21 | 0.14–0.15 | 24.66–111.26 | Zhu et al. (2017) |
| Average | 13.23 | 1.35 | 73.02 | 0.20 | 0.15 | 53.90 | Zhu et al. (2017) |
| Yinachang diorite | 14.8–16.3 | 2.5–5.9 | 17.2–28.8 | 1.4–1.9 | 0.3–0.6 | 4.9–7 | This study |
| Average | 15.6 | 4.2 | 23 | 1.6 | 0.4 | 5.9 | This study |
| Yinachang gabbro | 10.9–11 | 1–1.1 | 10.2–10.5 | 0.2 | 0.2 | 10–10.4 | This study |
| Average | 11 | 1.02 | 10.4 | 0.2 | 0.2 | 10.2 | This study |

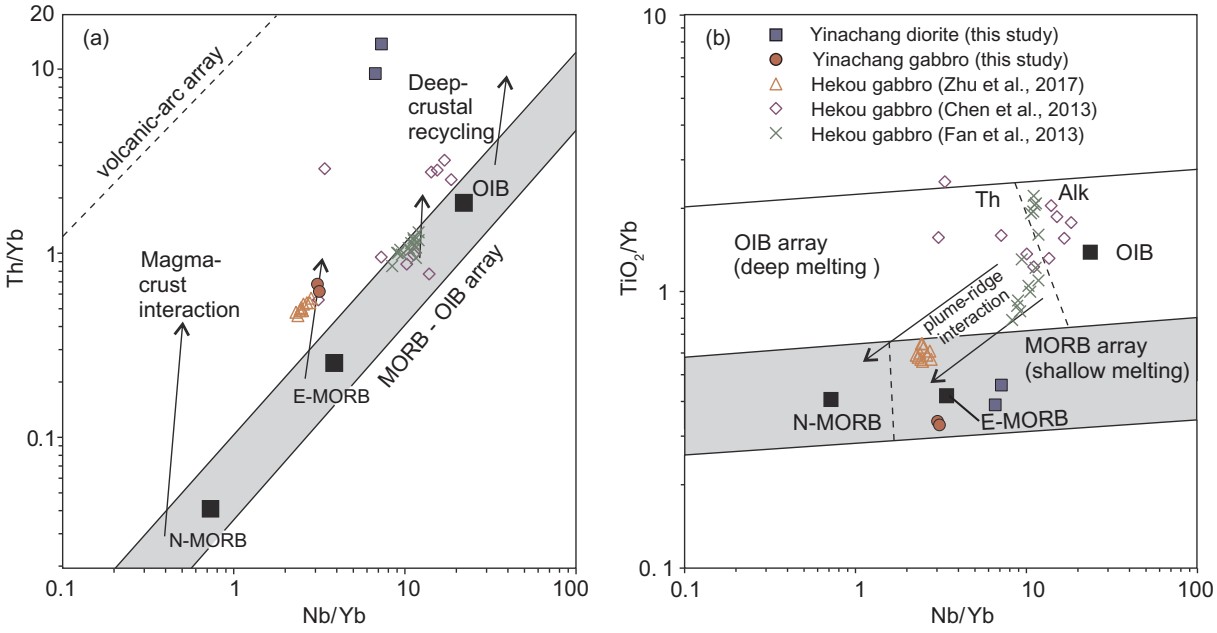


**Fig. 14.** Discrimination diagrams: (a) Nb/Yb vs Th/Yb plot for oceanic basalts (intra-plate islands, plume-distal ocean ridges and oceanic plateaux) forming a MORB–OIB array (shaded) with volcanic-arc basalts plotting above the array. Crustal-contaminated and alkalic basalts containing a large recycled crustal component plot above the MORB–OIB array, or along a vector at a steep angle to the array, reflecting selective Th addition; (b) Nb/Yb vs $TiO_2$/Yb diagram where OIBs have higher Ti/Yb ratios than MORBs reflecting deeper melting resulting from a combination of a thicker lithospheric cap and hotter mantle temperatures. Alkalic basalts within the OIB field, have the higher Nb/Yb and Ti/Yb ratios. Plume-distal ridges tend to produce N-MORB in the upper part of the MORB field, and plume-proximal ridges in the lower part of the MORB field. In regions of plume–ridge interaction (near-ridge plumes, ocean–continent transitions at volcanic-rifted margins), basalts follow a diagonal trend from the tholeiitic OIB to MORB array. Oceanic plateaus typically form clusters in the centre of the MORB array. Reference fields are from Pearce, 2008. Data are from Chen et al. (2013), Fan et al. (2013), Zhu et al. (2017), and this study.

geochemically similar to our gabbro samples (discussed further below). If the age of the mineralisation is ca. 1690 Ma, both the diorite and gabbro might be broadly coeval with the mineralisation in the Kangdian region and could have contributed to the heat source for the mineralised fluids with deposition of metals taking place during changes in pressure, temperature, and fluid chemistry. It is therefore proposed that the xenocrystic zircons in the diorite formed as part of the Columbia Supercontinent cycle, placing the study area in the Columbia Supercontinent.

### 6.2. Petrogenesis and the tectonic setting of the magma

The gabbro samples are unsaturated in silica, rich in Fe-Mg and $P_2O_5$, and have a high alkalinity, which are characteristic of tholeiitic basalt found in an oceanic island basalt (OIB) tectonic setting. Such basaltic rocks vary from tholeiitic to alkali basalt, but are never calc-alkaline and are typically located away from plate boundaries over hotspots or mantle plumes (e.g. Niu et al., 2011).

Both Th and Ta are strongly incompatible HSFEs, and their ratio can be indicative of the geochemical characteristics of the original magma of an igneous rock and can be used to show whether the magma was contaminated. Given that the primitive mantle's Th/Ta value is ~2.3 and that for the upper crust is ~10 (Wooden et al., 1993), the Th/Ta values of 3.04–3.32 for the Yinachang gabbro are indicative of a primordial mantle source, and the values of 17.21–21.07 for the diorite are indicative of a magma contaminated by the crust.

Geochemical heterogeneity of the Earth's mantle is revealed through isotopic measurements, and the trace element contents of OIB and MORB. Zindler and Hart (1986) suggest that the isotopic variability of the mantle is characterised by a spectrum with end-members represented by depleted MORB mantle (DMM), high 'μ' or high $^{238}U/^{204}Pb$ mantle (HIMU), enriched mantle '1' (EM1), and enriched mantle '2' (EM2). However, the petrologic characteristics of the mantle sources of these end-members are not well understood (Weaver, 1991; Hart et al., 1992). Trace element ratios can be used to distinguish between the primitive mantle, continental crust, and N-MORB sources of basalts with the characteristics of the DMM, EM1 and EM2 end-members. Furthermore, the ratios of REEs and LILES provide a limited characterisation of mantle material, because of their similar geochemistry, and weak fractionation in the mantle, but intensely fractionated HFSEs can help identify the source of OIB (e.g. Weaver, 1991). Using these geochemical criteria included in Table 4, the Yinachang gabbro has an EM1 OIB-type mantle source, and the Yinachang diorite has a mixed crustal and mantle source.

The Th/Yb vs Nb/Yb and $TiO_2$/Yb vs Nb/Yb diagrams in Fig. 14 show: (i) our Yinachang gabbro and diorite samples might have originated from an E-MORB-type magma and were variably contaminated by the crust; (ii) the plots of the Hekou gabbro samples of Chen et al. (2013) are scattered in Fig. 14 and might include different suites of gabbro or are variably altered; (iii) the Hekou gabbro samples of Fan et al. (2013) plot tightly in the OIB field in Fig. 14a, form a linear trend crossing the tholeiitic and alkali OIB field in Fig. 14b and might be plume-related; and (iv) the Hekou gabbro samples of Zhu et al. (2017) plot near those of our gabbro samples and near the crustal-contaminated E-MORB field in Fig. 14a and the E-MORB field in Fig. 14b. These plots show that the Hekou gabbro of Chen et al. (2013) and Fan et al. (2013) are not from the same unit as those from both Zhu et al. (2017) and our samples.

Similar patterns are present in Fig. 15a with the samples from Chen et al. (2013) being scattered and the samples from Fan et al. (2013) plotting in the P-MORB and arc-basalt (AB) fields. The ca. 1735 Ma gabbroic samples from Zhu et al. (2017) plot tightly in the E-MORB field near the boundary with the Island-Arc Tholeiite field, and our gabbro samples in the AB field. Additionally, our diorite samples plot in the Continental Margin to Volcanic Arc fields, which is different from our gabbroic samples that pot in the Rifted Margin and Ocean-Continent Transition fields (Fig. 15b). An implication of the geochemical similarity between the ca. 1735 Ma gabbro samples of Zhu et al. (2017)

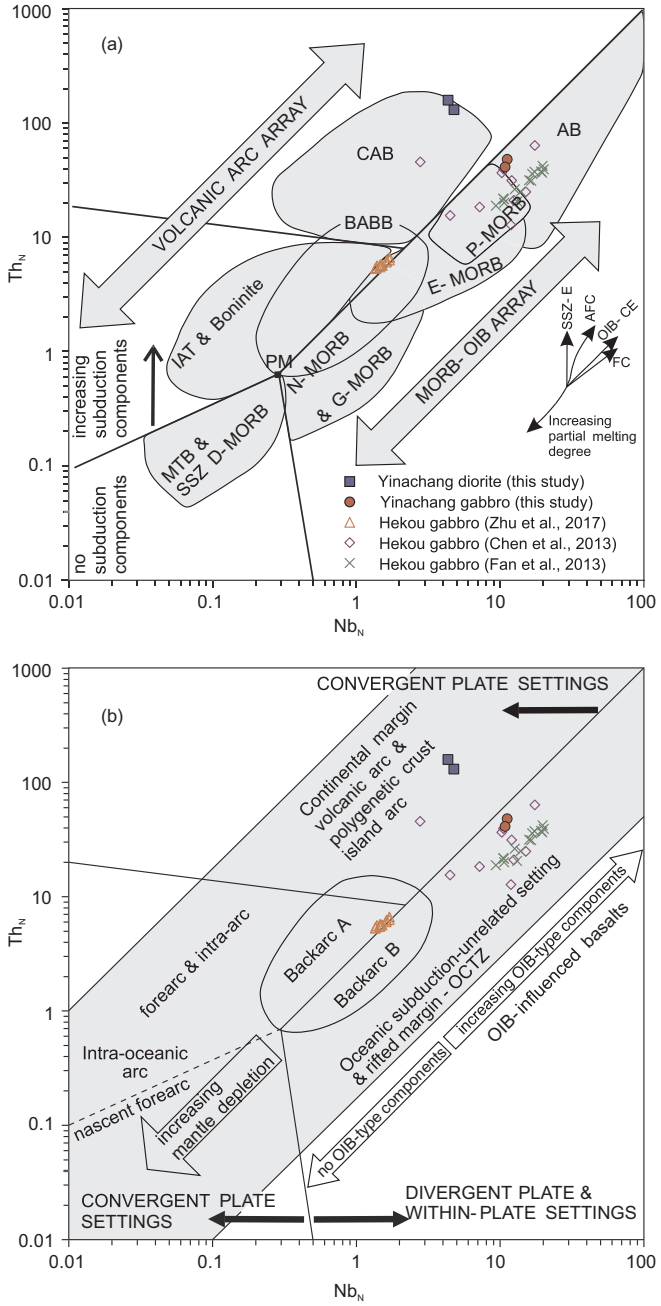


**Fig. 15.** Discrimination diagrams: (a) $Th_N$ vs $Nb_N$ diagram showing the compositional variations of different post-Archaean basaltic rock-types (vectors indicate the trends of compositional variations due to the main petrogenetic processes); and (b) $Th_N$ vs $Nb_N$ diagram showing the tectonic setting for basaltic types. "Back-arc A" is a back-arc basin basalt (BABB) characterised by input of subduction or crustal components (e.g. immature intra-oceanic or ensialic back-arcs), whereas "Back-arc B" indicates BABBs with no input of subduction or crustal components (e.g. mature intra-oceanic back-arcs). In both panels, Nb and Th are normalised to the N-MORB composition of Sun and McDonough (1989). Reference fields are from Saccani (2015). Data sources: Chen et al. (2013), Fan et al. (2013), Zhu et al. (2017), and this study. Abbreviations: SSZ-E = supra-subduction zone enrichment, AFC = assimilation-fractional crystallisation, OIB-CE = Ocean Island-type (plume-type) component enrichment, FC = fractional crystallisation, OCTZ = Ocean-Continent Transition Zone.

and ours is that our samples have a similar age of 1735 Ma.

### 6.3. Implications for ore genesis

The mineralisation in the Kangdian area took place near the rifted Palaeo- to Mesoproterozoic continental margin in a region that included many Fe-rich and structurally controlled volcanoes, which were accompanied by high-temperature fluids carrying elevated REEs from the mantle.

The pre-Tethyan Oceanic plate subducted beneath the western part of the Yangtze continental plate followed by discontinuous extensional movements related to the upwelling of a mantle plume resulting in the formation of a rift basin. The interaction of the plume with the lithospheric and lower continental crust led to the emplacement of diorite and gabbro in our study region. This was accompanied by a large volume of mineralised fluid containing metals such as Cu, Fe, Au, Mo, and U in response to changes in temperature, pressure, and fluid chemistry. The IOCG deposits were deposited in continental rift basins, accompanied by the fragmentation of the Palaeoproterozoic Columbia Supercontinent around 1735–1690 Ma. The REEs may be closely related to the large amount of alkali-rich magma formed during the fragmentation of the supercontinent.

The proposed model for the ore genesis and setting is summarised in Fig. 16, which illustrates the development of arc-related volcanism on a continental plate during subduction of an oceanic plate, and the rifting of a continental plate due to the presence of a mantle plume accompanied by the emplacement of intermediate to mafic plutonic rocks and deposition of the Yinachang Fe-Cu-Au-U-REE deposit.

## 7. Conclusions

The study area is in the Kangdian region in the southwestern part of the Yangtze Block of South China. Our study has shown that the age of the diorite at the Yinachang Fe-Cu-Au-U-REE deposit is younger than 2014 ± 30 Ma, but our gabbroic samples from the deposit could not be dated directly, because they are metamict resulting from their high uranium content. Nonetheless, given the similarity in the geochemistry of our samples and the ca. 1735 Ma Hekou gabbro, both our diorite and gabbro samples are probably similar in age to the Hekou gabbro.

The geochemistry of diorite and gabbro from the Yinachang deposit indicates that they were emplaced at temperatures between 700 and 1000 °C in an enriched Mid-Ocean Ridge and variably contaminated by crustal material. The tectonic setting was located at a rifted margin in the transition between the continental and oceanic crust. The alkaline magmatic rocks and REEs are closely related at the ca. 1690 Ma Yinachang deposit.

## Acknowledgements

This research was financially supported by the Major Basic Research Program of People's Republic of China (2014CB440903), by China Scholarship Council (201706400056), by the Fundamental Research Funds for the Central Universities, China University of Geosciences (Beijing) (Grant No. 2652017266), by the State Administration of Foreign Experts Affairs, China (Grant No. B07011), and by the MOST Special Fund from the State Key Laboratory of Geological Processes and Mineral Resources, China University of Geosciences. We are very grateful to Editor-in-Chief Franco Pirajno, and two reviewers for their constructive comments and assistance in improving the manuscript. We thank Guangzhi Meng, Chief Engineer of Geological Team 306 of Yunnan Non-ferrous Metals Geological Bureau, for his great support and assistance for our fieldwork. The authors acknowledge the facilities, and the scientific and technical assistance of the Australian Microscopy & Microanalysis Research Facility at the Centre for Microscopy, Characterisation & Analysis, The University of Western Australia, a facility funded by the University, State and Commonwealth

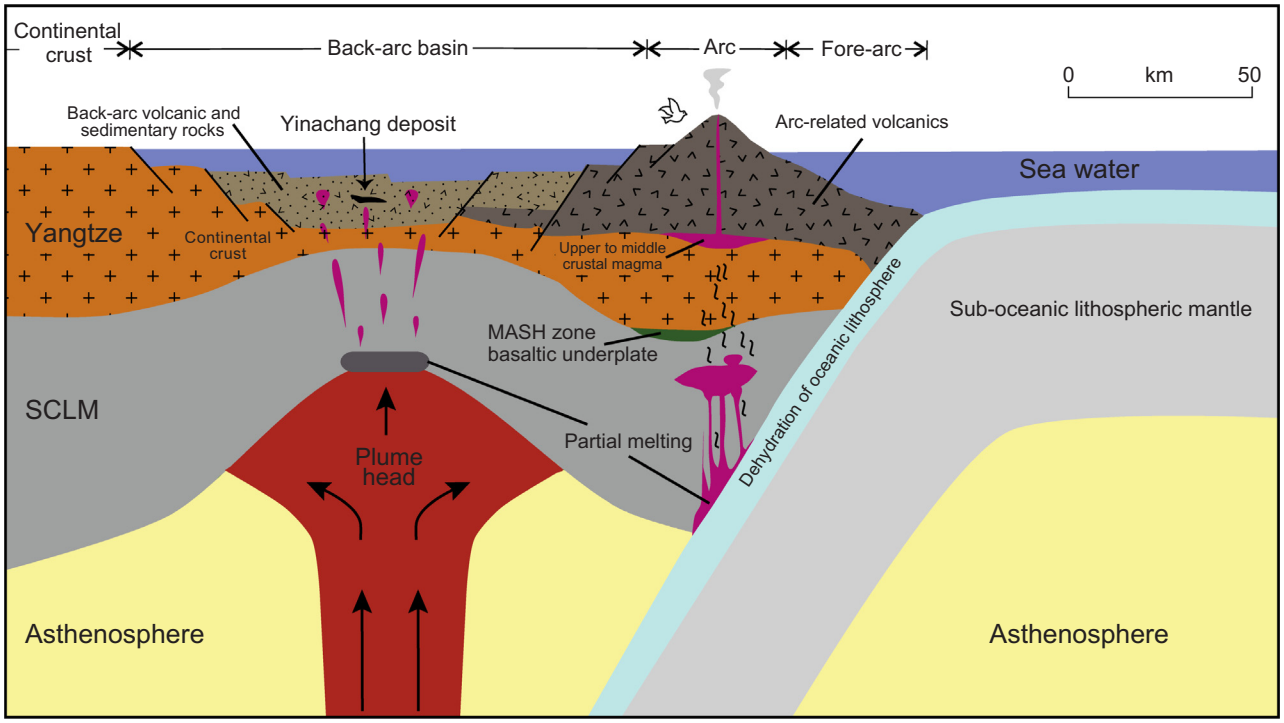


**Fig. 16.** Simplified cartoon showing regional tectonic setting of the Yinachang deposit in southwestern Yangtze Block (after Zhu et al., 2018).

Governments.

## Appendix A. Supplementary data

Supplementary data to this article can be found online at https://doi.org/10.1016/j.oregeorev.2018.11.005.

## References


Aldanmaz, E., Yaliniz, M.K., Güctekin, A., Göncüoğlu, M.C., 2008. Geochemical characteristics of mafic lavas from the Neotethyan ophiolites in western Turkey: implications for heterogeneous source contribution during variable stages of ocean crust generation. Geol. Mag. 145 (1), 37–54.

Andersen, T., 2002. Correction of common lead in U-Pb analyses that do not report $^{204}$Pb. Chem. Geol. 192 (1–2), 59–79.

Chang, X.Y., Zhu, B.Q., 2002. Isotope geochemistry of Dongchuan copper deposit, Yunnan, SW China: Stratigraphic chronology and application of lead Isotopes in geochemical exploration. Chin. J. Geochem. 21 (1), 65–72.

Chen, H.S., 1994. Isotope Geochemistry. Zhejiang University Press, Hangzhou, pp. 1–340 (in Chinese).

Chen, W.T., Zhou, M.F., Zhao, X.F., 2013. Late Paleoproterozoic sedimentary and mafic rocks in the Hekou Area, SW China: implication for the reconstruction of the Yangtze Block in Columbia. Precambrian Res. 231, 61–77.

Cherniak, D.J., Hanchar, J.M., Watson, E.B., 1997a. Rare earth diffusion in zircon. Chem. Geol. 134 (4), 289–301.

Cherniak, D.J., Hanchar, J.M., Watson, E.B., 1997b. Diffusion of tetravalent cations in zircon. Contrib. Mineral. Petrol. 127 (4), 383–390.

Cherniak, D.J., Watson, E.B., 2001. Pb diffusion in zircon. Chem. Geol. 172 (1–2), 5–24.

Cherniak, D.J., Watson, E.B., 2007. Ti diffusion in zircon. Chem. Geol. 242 (3–4), 470–483.

Corriveau, L., Mumin, A.H., 2010. Exploring for iron oxide copper-gold (Ag-Bi-Co-U) deposits: Case examples, classification and exploration vectors. Geol. Assoc. Can. Short Course Notes 20, 1–12.

Deng, X.H., Chen, Y.J., Santosh, M., Yao, J.M., 2013a. Genesis of the 1.76 Ga Zhaiwa Mo-Cu and its link with the Xiong'er volcanics in the North China Craton: implications for accretionary growth along the margin of the Columbia supercontinent. Precambrian Res. 227, 337–348.

Deng, X.H., Chen, Y.J., Santosh, M., Zhao, G.C., Yao, J.M., 2013b. Metallogeny during continental outgrowth in the Columbia supercontinent: Isotopic characterization of the Zhaiwa Mo-Cu system in the North China Craton. Ore Geol. Rev. 51, 43–56.

Evans, D.A.D., Mitchell, R.N., 2011. Assembly and breakup of the core of Paleoproterozoic-Mesoproterozoic Supercontinent Nuna. Geology 39 (5), 443–446.

Fan, H.P., Zhu, W.G., Li, Z.X., Zhong, H., Bai, Z.J., He, D.F., Chen, C.J., Cao, C.Y., 2013. 1.5 Ga mafic magmatism in south China during the break-up of the supercontinent Nuna/Columbia: The Zhuqing Fe–Ti–V oxide ore-bearing mafic intrusion in western Yangtze Block. Lithos 168–169, 85–98.

Fang, W.X., Yang, X.Y., Guo, M.H., Liu, Y.L., 2013. Relationships between alkaline Ti-Fe-Rich gabbros and iron-oxide-copper-gold deposits in the Baixila ore district, Yunnan. Geotect. Metal. 37 (2), 242–261 (in Chinese with English abstract).

Fang, W.X., 2014. Geotectonic evolution and the proterozoic iron oxide copper-gold deposits on the Western Margin of the Yangtze Massif. Geotect. Metal. 38 (4), 733–757 (in Chinese with English abstract).

Ferry, J.M., Watson, E.B., 2007. New thermodynamic M and revised calibrations for the Ti-in-zircon and Zr-in-rutile thermometers. Contrib. Mineral. Petrol. 154 (4), 429–437.

Gao, S., Ling, W.L., Qiu, Y.M., Lian, Z., Hartmann, G., Simon, K., 1999. Contrasting geochemical and Sm-Nd isotopic composition of Archean metasediments from the Kongling High-grade terrain of the Yangtze craton: evidence for cratonic evolution and redistribution of REE during crustal anataxis. Geochim. Cosmochim. Acta 63 (13–14), 2071–2088.

Geng, Y.S., Yang, C.H., Du, L.L., Wang, X.S., Ren, L.D., Zhou, X.W., 2007. Chronology and tectonic environment of the Tianbaohsan Formation: new evidence from zircon SHRIMP U-Pb age and geochemistry. Geol. Rev. 53 (4), 556–563 (in Chinese with English abstract).

Geng, Y.S., Liu, Y.Q., Gao, L.Z., Peng, N., Jiang, X.J., 2012. Geochronology of the Mesoproterozoic Tong'an Formation in southwestern margin of Yangtze craton: new evidence from zircon LA–ICP–MS U-Pb ages. Acta Geol. Sin. 86 (9), 1479–1490 (in Chinese with English abstract).

Greentree, M.R., Li, Z.X., Li, X.H., Wu, H.C., 2006. Late Mesoproterozoic to earliest neoproterozoic basin record of the Sibao orogenesis in Western South China and relationship to the assembly of Rodinia. Precambrian Res. 151 (1), 79–100.

Greentree, M.R., Li, Z.X., 2008. The oldest known rocks in south-western China: SHRIMP U-Pb magmatic crystallisation age and detrital provenance analysis of the Paleoproterozoic Dahongshan Group. J. Asian Earth Sci. 33, 289–302.

Grimes, C.B., John, B.E., Kelemen, P.B., Mazdab, F.K., Wooden, J.L., Cheadle, M.J., Hanghoj, K., Schwartz, J.J., 2007. Trace Element Chemistry of zircons from Oceanic Crust: A method for distinguishing detrital zircon provenances. Geology 35 (7), 643–646.

Groves, D.I., Bierlein, F.P., Meinert, L.D., Hitzman, M.W., 2010. Iron oxide copper-gold (IOCG) deposits through Earth history: implications for origin, lithospheric setting, and distinction from other epigenetic iron oxide deposits. Econ. Geol. 105, 641–654.

Guan, J.L., Zheng, L.L., Liu, J.H., Sun, Z.M., Cheng, W.H., 2011. Zircon SHRIMP U-Pb dating of Diabase from Hekou, Sichuan Province, China, and its geological significance. Acta Geol. Sin. 85 (4), 482–490 (in Chinese with English abstract).

Guo, Y., Wang, S.W., Sun, X.M., Liao, Z.W., Wang, Z.Z., Zhou, B.G., Yang, B., 2014a. Zircon U-Pb age of the Paleoproterozoic diabase from the Yinachang iron-copper deposit, Yunan Province, and its geological implication. Geotect. Metal. 38 (1), 208–215 (in Chinese with English abstract).

Guo, Y., Wang, S.W., Sun, X.M., Wang, Z.Z., Yang, B., Liao, Z.W., Zhou, B.G., Jiang, X.F., Hou, L., Yang, B., 2014b. The Paleoproterozoic breakup event in the southwest Yangtze block: evidence from U-Pb zircon age and geochemistry of diabase in Wuding, Yunnan Province, SW China. Acta Geol. Sin. 88 (9), 1651–1665 (in Chinese with English abstract).

Hart, S.R., Hauri, E.H., Oschmann, L.A., Whitehead, J.A., 1992. Mantle plumes and entrainment: isotopic evidence. Science 256, 517–520.

He, D.F., 2009. Petrological and geochemical characteristics of the Lala copper deposit in Sichuan Province. Unpublished Ph.D thesis, Institute of Geochemistry Chinese Academy of Sciences, Guiyang, pp. 1–84 (in Chinese with English abstract).
Hoskin, P.W.O., 2005. Trace-element composition of hydrothermal zircon and the alteration of Hadean zircon from the Jack Hills area, Australia. Geochim. Cosmochim. Acta 69 (3), 637–648.
Hou, L., Ding, J., Deng, J., Liao, Z.W., Peng, H.J., 2013. Zircon LA–ICP–MS dating of the magmatic breccia from the Yinachang iron–copper deposit in Wuding County of Yunnan Province and its geological significance. Geol. Bull. Chin. 32 (4), 580–588 (in Chinese with English abstract).
Hou, L., 2013. Proterozoic Fe–Cu–Au–REE metallogenic system of "Dongchuan" Group in central Yunnan province — A case study on the Yinachang deposit. Unpublished Ph.D thesis, China University of Geosciences (Beijing), Beijing, pp.1–179 (in Chinese with English abstract).
Hou, L., Peng, H.J., Ding, J., 2015a. Sources of the ore-forming materials for the Yinachang Fe–Cu–Au–REE deposit, Wuding, Yunnan Province: constraints from the ore geology and the S, Pb, H, O isotope geochemistry. Acta Petrol. Mineral. 34 (2), 205–218 (in Chinese with English abstract).
Hou, L., Ding, J., Deng, J., Peng, H.J., 2015b. Geology, geochronology, and geochemistry of the Yinachang Fe–Cu–Au–REE deposit of the Kangdian region of SW China: evidence for a Paleo-Mesoproterozoic tectono–magmatic event and associated IOCG systems in the western Yangtze Block. J. Asian Earth Sci. 103, 129–149.
Hu, A.Q., Zhu, B.Q., Mao, C.X., Zhu, N.J., Huang, R.S., 1991. Geochronology of the Dahongshan Group. Acta Geochim. 10 (3), 195–203.
Irvine, T.N., Barager, W.R., 1971. A guide to the chemical classification of the common volcanic rocks. Can. J. Earth Sci. 8, 523–548.
Joseph, G.M., Santosh, M., 2017. The Columbia supercontinent revisited. Gondwana Res. 50, 67–83.
Li, X.H., Li, Z.X., Li, W.X., Liu, Y., Yuan, C., Wei, G.J., Qi, C.S., 2007. U-Pb zircon, geochemical and Sr-Nd-Hf isotopic constraints on age and origin of Jurassic I- and A-type granites from central Guangdong, SE China: a major igneous event in response to foundering of a subducted flat-slab? Lithos 96 (1–2), 186–204.
Li, X.C., Zhao, X.F., Zhou, M.F., Chen, W.T., Cun, Z.Y., 2015. Fluid Inclusion and Isotopic Constraints on the Origin of the Paleoproterozoic Yinachang Fe-Cu-(REE) Deposit, Southwest China. Econ. Geol. 110, 1339–1369.
Li, Z.Q., Hu, R.Z., Wang, J.Z., Liu, J.J., Li, C.Y., Liu, Y.P., Ye, L., 2002. Lala Fe-Oxide-Cu-Au-U-REE ore deposit, Sichuan China–an example of superimposed mineralization. Bull. Miner. Petrol. Geochem. 21 (4), 258–260 (in Chinese with English abstract).
Ludwig, K.R., 2008. Isoplot 3.70: A Geochronological Toolkit for Microsoft Excel. Berkeley Geochronology Center Special Publication No.4, Berkeley, CA.
Middlemost, E.A.K., 1972. A simple classification of volcanic rocks. Bull. Volcanol. 36 (2), 382–397.
Middlemost, E.A.K., 1985. Magmas and Magmatic Rocks. Longman, London, pp. 1–266.
Middlemost, E.A.K., 1994. Naming materials in the magma/igneous rock system. Earth-Sci. Rev. 37 (3–4), 215–224.
Miller, C.F., McDowell, S.M., Mapes, R.W., 2003. Hot and cold granites? Implications of zircon saturation temperatures and preservation of inheritance. Geology 31 (6), 529–532.
Mou, C.L., Lin, S.L., Yu, Q., 2003. The U-Pb ages of the volcanic rock of the Tianbaoshan formation, Huili, Sichuan Province. J. Stratigr. 27 (3), 216–219 (in Chinese with English abstract).
Niu, Y., Wilson, M., Humphreys, E.R., O'Hara, M.J., 2011. The origin of intra-plate ocean island basalts (OIB): the lid effect and its geodynamic implications. J. Petrol. 52 (7–8), 1443–1468.
Pearce, J.A., 2008. Geochemical fingerprinting of oceanic basalts with applications to ophiolite classification and the search for Archean oceanic crust. Lithos 100, 14–48.
Peccerillo, R., Taylor, S.R., 1976. Geochemistry of Eocene calc-alkaline volcanic rocks from the Kastamonu area, Northern Turkey. Contrib. Mineral. Petrol. 58, 63–81.
Peng, M., Wu, Y.B., Wang, J., Jiao, W.F., Liu, X.C., Yang, S.H., 2009. Paleoproterozoic mafic dyke from Kongling terrain in the Yangtze craton and its implication. Chin. Sci. Bull. 54 (6), 1098–1104.
Peng, M., Wu, Y.B., Gao, S., Zhang, H.F., Wang, J., Liu, X.C., Gong, H.J., Zhou, L., Hu, Z.C., Liu, Y.S., Yuan, H.L., 2012. Geochemistry, zircon U-Pb age and Hf isotope compositions of Paleoproterozoic aluminous A-type granites from the Kongling Terrain, Yangtze Block: constraints on petrogenesis and geologic implications. Gondwana Res. 22 (1), 140–151.
Pesonen, L., Mertanen, S., Veikkolainen, T., 2012. Paleo-mesoproterozoic supercontinents-a paleomagnetic view. Geophysica 48 (1–2), 5–48.
Qian, J.H., Shen, Y.R., 1990. In: Dahongshan Volcanic Rock Type Iron and Copper Deposit in Yunnan Province. Geological Publishing House, Beijing, pp. 1–238 (in Chinese).
Qiu, Y.M., Gao, S., McNaughton, N.J., Groves, D.I., Ling, W.L., 2000. First evidence of > 3.2 Ga continental crust in the Yangtze craton of south China and its implication for Archean crustal evolution and Phanerozoic tectonics. Geology 28 (1), 11–14.
Rogers, J.W., Santosh, M., 2002. Configuration of Columbia, a Mesoproterozoic supercontinent. Gondwana Res. 5 (1), 5–22.
Saccani, E., 2015. A new method of discriminating different types of post-Archean ophiolitic basalts and their tectonic significance using Th-Nb and Ce-Dy-Yb systematics. Geosci. Front. 6 (4), 481–501.
Silveira, E.M., Soderlund, U., Oliveira, E.P., Ernst, R.E., Menezes Leal, A.B., 2012. First precise U-Pb baddeleyite ages of 1500 Ma mafic dykes from the Sao Francisco Craton, Brazil, and tectonic implication. Lithos 174, 144–156.
Sun, K.X., Shen, Y.R., Liu, G.Q., Li, Z.W., Pan, X.Y., 1991. In: The Iron and Copper Deposits of Proterozoic in the Middle of Yunnan. China University of Geosciences Press, Wuhan, pp. 1–169 (in Chinese).
Sun, S.S., McDonough, W.F., 1989. Chemical and isotopic systematics of oceanic basalts: Implications for mantle composition and processes. In: Saunders, A.D., Norry, M.J. (Eds.), Magmatism in Ocean Basins. Geological Society Special Publications 42, London, pp. 313–345.
Sun, Z.M., Yin, F.G., Guan, J.L., Liu, J.H., Li, J.M., Geng, Q.R., Wang, L.Q., 2009. SHRIMP U-Pb dating and its stratigraphic significance of tuff zircons from Heishan Formation of Kunyang Group, Dongchuan area, Yunnan Province, China. Geol. Bull. China 28 (7), 896–900 (in Chinese with English abstract).
Wang, X.L., Zhou, J.C., Qiu, J.S., Zhang, W.L., Liu, X.M., Zhang, G.L., 2006. LA-ICP-MS U-Pb zircon geochronology of the Neoproterozoic igneous rocks from northern Guangxi, South China: implications for tectonic evolution. Precambrian Res. 145 (1–2), 111–130.
Wang, D.B., Yin, F.G., Sun, Z.M., Wang, L.Q., Wang, B.D., Liao, S.Y., Tang, Y., Ren, G.M., 2013a. Zircon U-Pb age and Hf isotope of Paleoproterozoic mafic intrusion on the western margin of the Yangtze Block and their implications. Geol. Bull. China 32 (4), 617–630 (in Chinese with English abstract).
Wang, S.W., Liao, Z.W., Sun, X.M., Jian, X.F., Zhou, B.G., Guo, Y., Luo, M.J., Zhu, H.P., Ma, D., 2013b. Geochemistry of Paleoproterozoic diabases in the Dongchuan copper deposit, Yunnan, SW China: response to break up of the Columbia supercontinent in the southwestern margin of Yangtze block. Acta Geol. Sin. 87 (12), 1834–1852 (in Chinese with English abstract).
Wang, Z.Z., Guo, Y., Yang, B., Wang, S.W., Sun, X.M., Hou, L., Zhou, B.G., Liao, Z.W., 2013c. Discovery of the 1.73 Ga Haizi anorogenic type granite in the western margin of Yangtze craton and its geological significance. Acta Geol. Sin. 87 (7), 931–942 (in Chinese with English abstract).
Watson, E.B., Harrison, T.M., 1983. Zircon saturation revisited: temperature and composition effect in a variety of crustal magmas types. Earth Planet. Sci. Lett. 64, 295–304.
Watson, E.B., Harrison, T.M., 2005. Zircon thermometer reveals minimum melting conditions on earliest earth. Science 308, 841–844.
Watson, E.B., Wark, D.A., Thomas, J.B., 2006. Crystallization Thermometers for Zircon and Rutile. Contrib. Mineral. Petrol. 151 (4), 413–433.
Weaver, L.W., 1991. The origin of ocean island basalt end–member composition: trace element and isotopic constrains. Earth Planet. Sci. Lett. 104, 381–397.
Williams, P.J., Barton, M.D., Johnson, D.A., Fontboté, L., De Haller, A., Mark, G., Oliver, N.H.S., Marschik, R., 2005. Iron Oxide Copper-gold Deposits: Geology, Space-time Distribution and Possible Modes of Origin. Economic Geology 100th Anniversary Volume, pp. 371–405.
Wooden, J.L., Czamanske, G.K., Fedorenko, V.A., Arndt, N.T., Chauvel, C., Bouse, R.M., King, B.W., Knight, R.J., Siems, D.F., 1993. Isotopic and trace–element constraints on mantle and crustal contributions to Siberian continental flood basalts, Noril'sk area, Siberia. Geochim. Cosmochim. Acta 57, 3677–3704.
Wu, J.M., Liu, Z.C., Li, G.J., 1998. In: The Copper Deposits in West of the Yangtze Block. China University of Geosciences, Wuhan, pp. 1–271 (in Chinese).
Yang, H., Liu, F.L., Du, L.L., Liu, P.H., Wang, F., 2012. Zircon U-Pb dating for metavolcanites in the Laochanghe Formation of the Dahongshan Group in southwestern Yangtze Block, and its geological significance. Acta Petrol. Sin. 28 (9), 2994–3014 (in Chinese with English abstract).
Yang, H., Liu, P.H., Meng, E., Wang, F., Xiao, L.L., Liu, C.H., 2014. Geochemistry and its tectonic implications of metabasite in the Dahongshan Group in southwestern Yangtze block. Acta Petrol. Sin. 30 (10), 3021–3033 (in Chinese with English abstract).
Yang, Y.M., Tu, G.Z., Hu, R.Z., 2004. REE geochemistry of Yinachang Fe–Cu–REE deposit in Yunnan Province. Acta Miner. Sin. 24 (3), 301–308 (in Chinese with English abstract).
Yang, Y.M., Tu, G.C., Hu, R.Z., Shi, X.F., 2005. Sm–Nd isotopic geochronology of the Yinachang Fe–Cu–REE deposit at Wuding, Yunnan Province and its genetic significance. Chin. Sci. Bull. 50 (12), 1253–1258 (in Chinese with English abstract).
Ye, L., Liu, Y.P., Li, C.Y., Liu, J.J., 2004. Ar–Ar isotopic age Yinachang copper deposit, Wuding, Yunnan Province, China, and its implications. Acta Miner. Sin. 24 (4), 411–414 (in Chinese with English abstract).
Ye, X.T., Zhu, W.G., Zhong, H., He, D.F., Ren, T., Bai, Z.J., Fan, H.P., Hu, W.J., 2013. Zircon U-Pb and chalcopyrite Re–Os geochronology, REE geochemistry of the Yinachang Fe–Cu–REE deposit in Yunnan Province and its geological significance. Acta Petrol. Sin. 29 (4), 1167–1186 (in Chinese with English abstract).
Zhang, C.H., Gao, L.Z., Wu, Z.J., Shi, X.Y., Yan, Q.R., Li, D.J., 2007. SHRIMP U-Pb Zircon age of Tuff from the Kunyang Group in Central Yunnan: evidence for Grenvillian Orogeny in South China. Chin. Sci. Bull. 52 (11), 1517–1525.
Zhang, S.B., Zheng, Y.F., Wu, Y.B., Zhao, Z.F., Gao, S., Wu, F.Y., 2006. Zircon U-Pb age and Hf–O isotope evidence for Paleoproterozoic metamorphic event in South China. Precambrian Res. 151 (3–4), 265–288.
Zhang, S., Li, Z.X., Evans, D.A.D., Wu, H., Li, H., Dong, L., 2012. Pre-Rodinia supercontinent Nuna shaping up: a global synthesis with new paleomagnetic results from North China. Earth Planet. Sci. Lett. 353–354, 145–155.
Zhao, G.C., Cawood, P.A., Wilde, S.A., Sun, M., 2002. Review of global 2.1–1.8 Ga origins: Implications for a pre-Rodinia supercontinent. Earth-Sci. Rev. 59 (1–4), 125–162.
Zhao, G.C., Sun, M., Wilde, S.A., Li, S.Z., 2004. A Paleo-Mesoproterozoic supercontinent: assembly, Growth and breakup. Earth-Sci. Rev. 67 (1/2), 91–123.
Zhao, X.F., Zhou, M.F., Li, J.W., Sun, M., Gao, J.F., Sun, W.H., Yang, J.H., 2010. Late Paleoproterozoic to early Mesoproterozoic Dongchuan Group in Yunnan, SW China: implications for tectonic evolution of the Yangtze block. Precambrian Res. 182, 57–69.
Zhao, X.F., Zhou, M.F., 2011. Fe–Cu deposits in the Kangdian region, SW China: a proterozoic IOCG (iron–oxide–copper–gold) metallogenic province. Miner. Depos. 46, 731–747.
Zhao, X.F., Zhou, M.F., Hitzman, M.W., Li, J.W., Bennett, M., Meighan, C., Anderson, E., 2012. Late Paleoproterozoic to Early Mesoproterozoic Tangdan sedimentary rock–-hosted strata–bound copper deposit, Yunnan Province, Southwest China. Econ. Geol.

107 (2), 357–375.
Zhao, X.F., Zhou, M.F., Li, J.W., Selby, D., Li, X.H., Qi, L., 2013a. Sulfide Re–Os and Rb–Sr isotopic dating of the Kandian IOCG metallogenic province, SW China: implications for regional metallogenesis. Econ. Geol. 108, 1489–1498.
Zhao, X.F., Zhou, M.F., Li, J.W., Qi, L., 2013b. Late Paleoproterozoic sedimentary rock–hosted stratiform copper deposits in South China: Their possible link to the supercontinent Cycle. Miner. Depos. 48 (1), 129–136.
Zhao, X.F., Zhou, M.F., Gao, J.F., Li, X.C., Li, J.W., 2015. In situ Sr isotope analysis of apatite by LA–MC–ICPMS: constraints on the evolution of ore fluids of the Yinachang Fe–Cu–REE deposit, Southwest China. Miner. Depos. 50, 871–884.
Zhou, M.F., Zhao, X.F., Chen, W.T., Li, X.C., Wang, W., Yan, D.P., Qiu, H.N., 2014. Proterozoic Fe–Cu metallogeny and supercontinental cycles of the southwestern Yangtze Block, southern China, and northern Vietnam. Earth-Sci. Rev. 139, 59–82.
Zhou, J.Y., Mao, J.Y., Liu, F.Y., Tan, H.Q., Shen, B., Zhu, Z.M., Chen, J.B., Luo, L.P., Zhou, X., Wang, Y., 2011. SHRIMP U-Pb zircon chronology and geochemistry of albitite from the Hekou group in the western Yangtze block. J. Mineral. Petrol. 31 (3), 66–73 (in Chinese with English abstract).
Zhu, H.P., Zhou, B.G., Wang, S.W., Luo, M.J., Liao, Z.W., Guo, Y., 2011. Detrital zircon U-Pb dating by LA–ICP MS and its geological significance in western margin of Yangtze terrane. J. Mineral. Petrol. 31 (1), 70–74 (in Chinese with English abstract).
Zhu, W.G., Bai, Z.J., Zhong, H., Ye, X.T., Fan, H.P., 2017. The origin of the c. 1.7 Ga gabbroic intrusion in the Hekou area, SW China: constraints from SIMS U-Pb zircon geochronology and elemental and Nd isotopic geochemistry. Geol. Mag. 154 (2), 286–304.
Zhu, Z.M., Tan, H.Q., Liu, Y.D., 2018. Late Palaeoproterozoic Hekou Group in Sichuan, Southwest China: geochronological framework and tectonic implications. Int. Geol. Rev. 60 (3), 305–318.
Zindler, A., Hart, S., 1986. Chemical Geodynamics. Annu. Rev. Earth Plant. Sci. 141 (1), 493–571.